minerals

MDPI

Article

Detrital Zircon U-Pb Geochronology and Hf Isotope Geochemistry of the Hayang Group, SE Korea and the Himenoura and Goshoura Groups, SW Japan: Signs of Subduction-Related Magmatism after a Long Resting Period

Tae-Ho Lee [1] and Kye-Hun Park [2,*]

1 Geology Division, Korea Institute of Geoscience and Mineral Resources, Daejeon 34132, Korea; thlee80@kigam.re.kr
2 Department of Earth and Environmental Sciences, Pukyong National University, Busan 48513, Korea
* Correspondence: khpark@pknu.ac.kr; Tel.: +82-51-629-6629

Received: 1 September 2020; Accepted: 19 October 2020; Published: 22 October 2020

check for updates

Abstract: There was a hiatus in magmatism in Korea and Japan, located on the eastern continental margin of Asia, during a period of about 40 Ma from 160 Ma to 120 Ma. The cause of the resumption of magmatism since then is not yet well understood. In this study, we analyzed the Hf isotope composition of detrital zircons in the Cretaceous sediments of Korea (Hayang Group) and Japan (Goshoura and Himenoura groups) to investigate the tectonic evolution of eastern Asia in the Early Cretaceous period. $\varepsilon_{Hf}(t)$ in Cretaceous zircons from Japanese samples values from +8.2 to +0.1, suggesting that magmatism was sourced from the depleted juvenile materials, which is compatible with ridge subduction and subsequent melting of the young oceanic crust. $\varepsilon_{Hf}(t)$ values from Cretaceous zircons in the Hayang Group are negative, except for the Jindong Formation, which had a sediment supply from Japan, indicating that the old continental crust material of the Korean Peninsula was included in the magma generation. The detrital zircons of this study exhibit a depleted isotopic character at the beginning of subduction-related magmatism in Permian and Early Cretaceous, and then gradually change to a more enriched composition. This trend may be a typical example of the Pacific-type orogenic cycle.

Keywords: Gyeongsang Basin; Goshoura Group; Himenoura Group; detrital zircon; Hf isotope; U-Pb age; ridge subduction; Pacific-type orogen

1. Introduction and General Geology

The assembly of continental fragments in East Asia appears to have been completed during the Early Triassic period, when there was a continental collision between North China and South China blocks [1,2]. In the process of assembling continental fragments such as South China Block, North China Block, and Japanese Islands in this region, the Paleo-Pacific plates to the east have subducted below them and have triggered various tectonic activities and tectono-magmatic processes, including subduction-related magmatism [3–5], metamorphism [6–8], and terrestrial basin formation [9–11]. However, in the eastern margin of the Eurasia continent, especially in Japanese islands, igneous activities related to subduction of the Paleo-Pacific plate are observed even long before its complete assembly. The Japanese Islands have been affected by the subduction of Paleo-Pacific plates since about 500 Ma [12]. Since this time, there were several cyclic igneous activities called Pacific-type orogeny, and arc-related pull-apart sedimentary basins developed within the Japanese Islands [5,13]. As a result, the Japanese islands today consist mainly of tectonic units such as Paleozoic to Cenozoic accretionary complexes, high-pressure metamorphic belts, granite batholith suits, and sedimentary basins [5].

During the Phanerozoic subduction of Paleo-Pacific plates in the East Asian continental margin formed tectonic cycles repeated several times. It has been suggested that each cycle begins with an ocean ridge subduction (e.g., the Renge (Carboniferous), Farallon (Triassic), Izanagi (early Cretaceous), and Kula (late Cretaceous) [5]). The subduction of the Izanagi plate produced coeval Cretaceous orogenic components such as the Sanbagawa high-pressure metamorphic belt, the Sanbosan accretionary complex, the Ryoke-Sanyo batholith belt, and several sedimentary basins [13–15]. When each of these cycles begins and ends, and what characteristics do each of these cycles have over time is important in understanding these tectonic cycles. For example, the Mesozoic magmatism in Korea and Japan had a quiescent period from about 160 Ma to about 120 Ma [16–18].

The detrital zircons in sediments are suitable for studying the history of magmatism because they can comprehensively sample magmatism in the sediment source area and thus record the petrologic history of an arc. The detrital zircons of the Cretaceous basins of the Korean peninsula and Japanese islands, created by tectonic regime change during the Early Cretaceous period, are thought to be recording these changes in tectonic settings and magmatism [11,19,20]. The U-Pb age and Hf isotopic data of the detrital zircon can be used to trace the origin of the sediments, to limit the maximum deposition time, and to trace the tectonic environment and source materials of the magma-generated magma [21]. This study attempts to find out the temporal distribution of magmatism before the sedimentation by finding the distribution of U-Pb ages from the detrital zircons of the Cretaceous sediments in these regions, i.e., the Hayang Group in the southeastern Korean peninsula and Himenoura and Goshoura Group in SW Japan. From this, we verify the resumption period of early Cretaceous subduction-related magmatism, and also attempt to clarify the characteristics and tectonic settings of magmatism in that period through Hf isotope analysis of these zircons.

Sedimentary basins were produced in many places in Korea and Japan in the Cretaceous Period. The largest of these is the Gyeongsang Basin in the southeastern part of the Korean peninsula and consists of Sindong, Hayang, and Yucheon groups from the bottom. The Gyeongsang Basin was produced as a terrestrial back-arc basin [9]. No evidence of igneous activity in the early stages of basin formation was found, but detrital zircons with an age of about 128 Ma were found in the Nakdong Formation, the lowest layer, limiting the timing of basin formation [11]. Compared to the Sindong Group, where the detrital zircons of the Cretaceous age rarely appear, the overlying Hayang Group includes a high proportion of Cretaceous age zircons, especially those from about 120–110 Ma [19]. This indicates that there was enhanced igneous activity from this period and the tectonic environment gradually changed to intra-arc [19]. Cretaceous basins exist in several places in Southwest Japan. Among them, the Kanmon Group in Kyushu seems to have provenance of much of the sediment in the Korean Peninsula [22], suggesting that it was linked to Gyeongsang Basin at the time of deposition. The Cretaceous basins in Kyushu, unlike Korea, exhibit the characteristics of marine basins. However, there is evidence that sediments originated from the Korean Peninsula as detrital zircons include Paleoproterozoic ages, which are not present in Japan but characteristic of Precambrian basement rocks on the Korean Peninsula [22].

The Upper Cretaceous Himenoura Group and Geoshoura Group are distributed throughout the region including the Amakusa Islands, Kosikijima Islands, and the Uto Peninsulain in the western side of Kyushu (Figure 1) [23–25]. The basement rocks of Amakusa Island and the Uto Peninsula consist mainly of Cretaceous Higo plutonic-metamorphic rocks and Nagasaki metamorphic rocks [24]. The unconformably overlying rocks are composed of the Cretaceous Goshoura Group, Himenoura Group, Paleogene Miroku Group, Hondo Group, Sakasegawa Group, Neogene Kunhinotsu Group, and Paleogene to Neogene granitoids intruding into them. The Goshoura group is mainly distributed on the islands of Goshoura and Shishijima, which is the eastern part of the Amakusa Islands, and unconformably overlies the Higo Granitoids. The Goshoura Group is divided into Eboshi, Enokuchi, and Karakizaki formations in ascending order and consists of pebble bearing sandstone, sandstone and mudstone. Depositional environments of the Goshoura Group vary from terrestrial to marine deposits (e.g., floodplain, intertidal zone, and continental shelf) because of effects on sea-level fluctuation caused by repeated transgression and regression. Abundant mollusk fossils such as ammonite and bivalve have been reported from this group, suggesting that the sedimentation of the Goshoura Group ranges from Albian to Cenomanian [26,27].

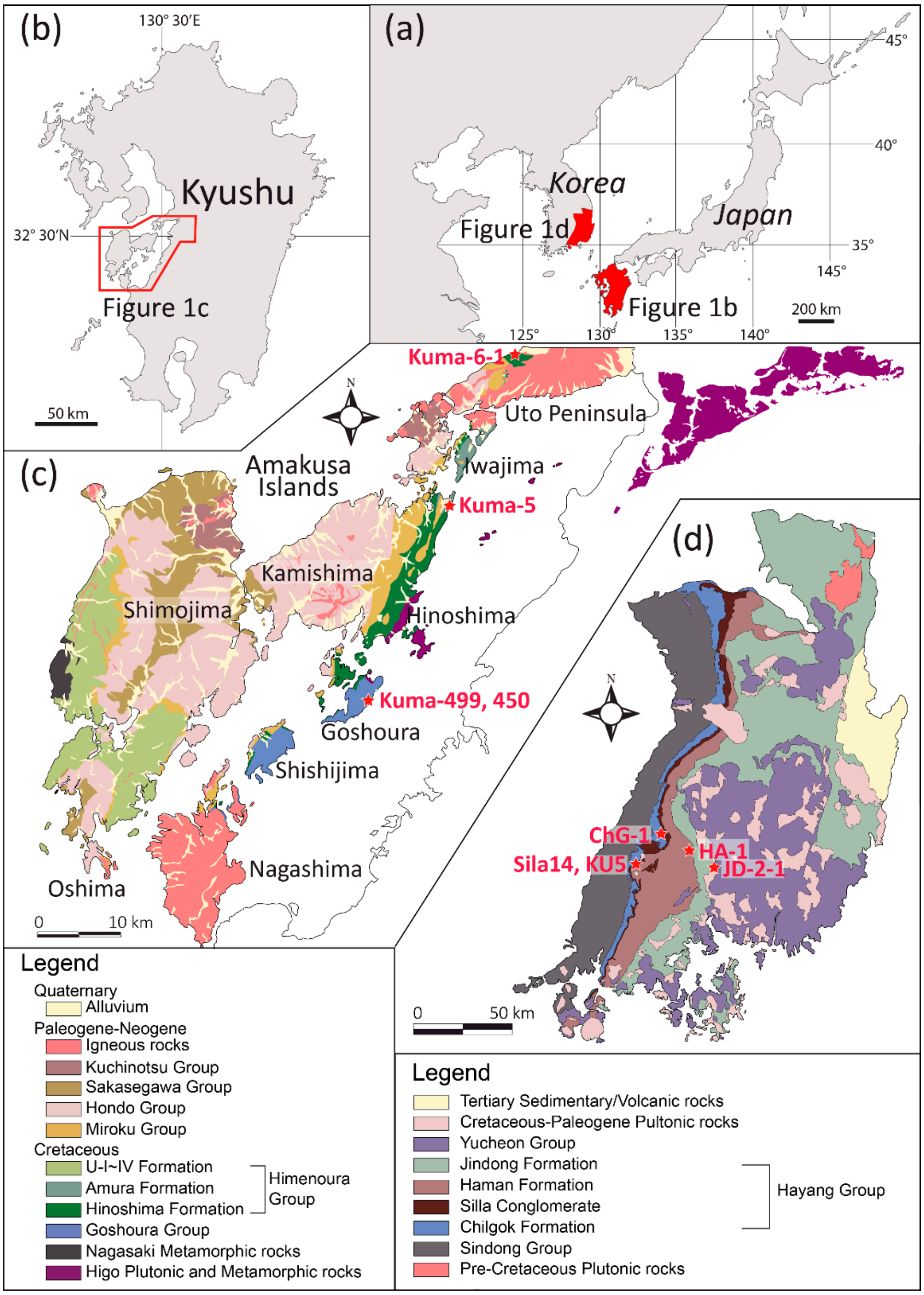

Figure 1. Geological map of the Gyeongsang basin in southeastern Korea (after Lee et al. 2018) [19] and the Amakusa Islands (after Saito et al. 2010) [23] with sample locations. (**a**) East Asia map including Korea and Japan. The positions of Kyushu and the Gyeongsang Basin are marked in red. (**b**) The inset within Kyushu marks the location of the Amakusa Islands and Uto Peninsula, where the Cretaceous Himenoura and Goshoura groups are distributed. (**c**) The distribution of the Cretaceous Himenoura and Goshoura groups and sampling locations from them are shown. (**d**) It is a schematic geological map of the Cretaceous Gyeongsang basin and also shows the sampling locations in the Hayang Group.

The Himenoura Group extends from northeast to southwest and is exposed to the northeast of the Amakusa Islands. It is unconformable overlying the Higo plutonic and metamorphic rocks and the Goshoura Group and unconformably overlained by the Paleogene Miroku Group. The Himenora group is divided into lower subgroup and upper subgroup, the former consists of the lower Hinoshima Formation and the upper Amura Formation, and the latter consists of four formations from the U-I layer to the U-IV layer. Lower Hinoshima Formation is characterized by sedimentation of fining-upward sequences consisting of conglomerate, sandstone and mudstone, and upper Amura Formation is characterized by alternation of mudstone and sandstone. The Himenoura Group shows a variety of sedimentary environments from shallow marine to continental slopes and as well as pelagic deposits. In addition, the sedimentary environmental characteristics of the incised valleys have been reported from the lower part. Diverse fossils such as foraminiferas, radiolarians, ammonoids, and inoceramids have been found from the Himenoura Group, suggesting ages from Santonian to Campanian [28,29]. Recent zircon U-Pb age determination from felsic tuffs and suggested that the depositional ages of Hinoshima and Amura Formation were 85.4 ± 1.3 Ma (n = 15, MSWD = 0.83) and 81.5 ± 1.1 Ma (n = 20, MSWD = 1.3), respectively [25].

The Gyeongsang Basin is a Cretaceous non-marine sedimentary basin located southeast of the Korean peninsula (Figure 1). The west and north of the Gyeongsang Basin are surrounded by the Yeongnam Massif consisting of Paleoproterozoic metamorphic rocks and Mesozoic granitoids that intrude them. The east and south of the Gyeongsang basin face the sea. The Cretaceous Gyeongsang Supergroup deposited in the Gyeongsang basin consists of Sindong, Hayang, and Yucheon groups in ascending order [30]. The Hayang Group of the Miryang sub-basin is composed of Chilgok Formation, Silla Conglomerate, Haman Formation, and Jindong Formation in ascending order [31]. These formations were deposited in either alluvial, fluvial, or lacustrine environments [32]. In the lower layers of the Gyeongsang Basin, sediments were supplied by waters flowing from the west and northwest [33–36], but sediments constituting the upper layers were supplied from streams flowing from the east, the direction of the Japanese islands connected to the Korean Peninsula at the time [32,37–39]. The maximum depositional ages of the four formations constituting the Hayang Group defined from the youngest U-Pb age populations of detrital zircons are as follows; 109 Ma for the Chilgok Formation, 106 Ma for the Silla Conglomerate, 105 Ma for the Haman Formation, and 100 Ma for the Jindong Formation [19].

2. Samples and Analytic Methods

In this study, the hafnium isotopic compositions of detrital zircons were analyzed to study the characteristics of the subduction-related igneous activity resumed in the Cretaceous period. Therefore, samples were selected for sedimentary layers that are expected to have many detrital zircons of Cretaceous age. For the Gyeongsang Basin in Korea, we used the Hayang Group samples whose detrital zircon U-Pb ages have already been reported [19]; two in the Silla Conglomerate (Sila14, KU5) and one in each of the Chilgok (CG-1), Haman (HA-1), and Jindong (JD-2-1) Formations. For U-Pb age measurement and Hf isotope analysis, we used two sandstone samples from the upper Cretaceous Himenoura Group (Kuma-5, Kuma-6-1) and two samples from the mid Cretaceous Goshoura Group (Kuma-449 and Kuma-450), Kyushu, SW Japan, collected during the IGCP-507 field trip (Figure 1) [24]. Two samples of the Goshoura Group (Kuma-499, 450) were collected from a quarry on Goshoura Island. Sample Kuma-6 was collected from the lower Hinoshima Formation of the Himenoura group of the Uto Peninsula. The Kuma-5 sample was taken from the upper Amur Formation of the Himenoura Group on Kamishima Island.

U-Pb age determination of zircons separated from four samples of the Himenoura and Goshoura groups was conducted using Sensitive High-Resolution Ion Micro Probe (SHIRMP-IIe/Mc) operated by Korea Basic Science Institute (KBSI). For the SHRIMP U-Pb age determination, the O_2^- primary ion beam was used with diameter of about 25 μm and beam current of 2.0–4.0 nA. Zircon standards SL13 (U 238 ppm) and FC-1 (1099 Ma) [40] were used for uranium concentration and age calibration, respectively. All uncertainties for individual analysis points in the data table are quoted at one sigma level. Data reduction was performed using the SQUID 2.5 program [41]. Tera-Wasserburg diagrams, condordia ages, age histograms, and probability density plots were constructed using Isoplot 3.71 [42]. The ^{207}Pb correction method was applied for ^{206}Pb/^{238}U ages below 1000 Ma, and the ^{204}Pb correction method was applied for ^{207}Pb/^{206}Pb ages greater than 1000 Ma.

Hf isotope data for zircons were obtained from the same analysis spots as the U-Pb age measurements. Hf isotope composition was measured in KBSI using a Nu Plasma II multi collector inductively coupled plasma mass spectrometer equipped with a New Wave Research 193 nm ArF excimer ablation system (LA-MC-ICPMS). For Hf isotope analysis, 10 Faraday collectors were set up for simultaneous detection of Hf-Lu-Yb isotopes. Instrument parameters and operating conditions include spot size 50 μm, 10 Hz repetition rate, and energy density of 6–8 J/cm^2. He (650 mL/min) and N_2 (2 mL/min) were used as carrier gases for high Hf isotope intensity [43]. The spot depth in Hf isotope analysis is in the range of 15–30 μm. To monitor the measured isotope ratios, we used a time-resolved analytical (TRA) procedure. Signal intensities for each collector were collected every 0.2 s integration time. Background intensity, dwell time, and wash out time were measured for 35 s, 60 s, and 15 s, respectively. The isobaric interferences of ^{176}Lu and ^{176}Yb for the ^{176}Hf signals were corrected using Chu et al. [44] and Vervoort, Patchett, Soderlund, and Baker [45]. The mass bias of the measured Hf isotope ratio was corrected to ^{179}Hf/^{177}Hf = 0.7325 using the exponential correction law [46]. All individual analyzes were calculated with 2-sigma uncertainty and data reduction was conducted with the Iolite 2.5 software program [47].

3. Results

3.1. U-Pb Age of the Detrital Zircons from the Himenoura and Goshoura Groups

Most of the detrital zircons separated from the sandstones of the Himenoura Group and the Goshoura Group of SW Japan except for one sample (Kuma-5) have crystal shapes of euhedral to subhedral with well-developed oscillatory growth zoning with no evidence of pre-Cretaceous zircon or old cores in CL images (Figure 2).

The U-Pb ages for 90 analytical spots for 85 zircon grains from the Himenoura Group and Goshoura Group of SW Japan are shown in Table A1 and Figure 3. Most zircon grains yield concordant or slightly discordant U-Pb ages. In the samples other than one (Kima-5), each single concordia age was obtained. The two samples of the Goshoura Group (Kuma-449, 450) yield concordia ages of 110.3 ± 0.7 Ma (n = 32, MSWD = 3.1) and 116.8 ± 0.8 Ma (n = 15, MSWD = 2.6), respectively. The lower Hinoshima Formation sample (Kuma-6) of the Himenoura group yields a concordant age of 114.9 ± 0.9 Ma (n = 12, MSWD = 1.4). Unlike these, the upper Amura Formation sample (Kuma-5) of the Himenoura group yields a wide range of ages from ca 2360 Ma to 86 Ma. The concordia ages of 88.4 ± 1.3 Ma (n = 6, MSWD = 0.1), 95.8 ± 1.6 Ma (n = 4, MSWD = 1.2), and 254.3 ± 1.8 Ma (n = 3, MSWD = 1.2) were obtained from the sample Kuma-5. Of the four samples analyzed from the Himenoura Group and Goshoura Group, only Kuma-5 has detrital zircons with ages other than Cretaceous, including Jurassic, Triassic, Permian, and Paleoproterozoic ones (Figure 4).

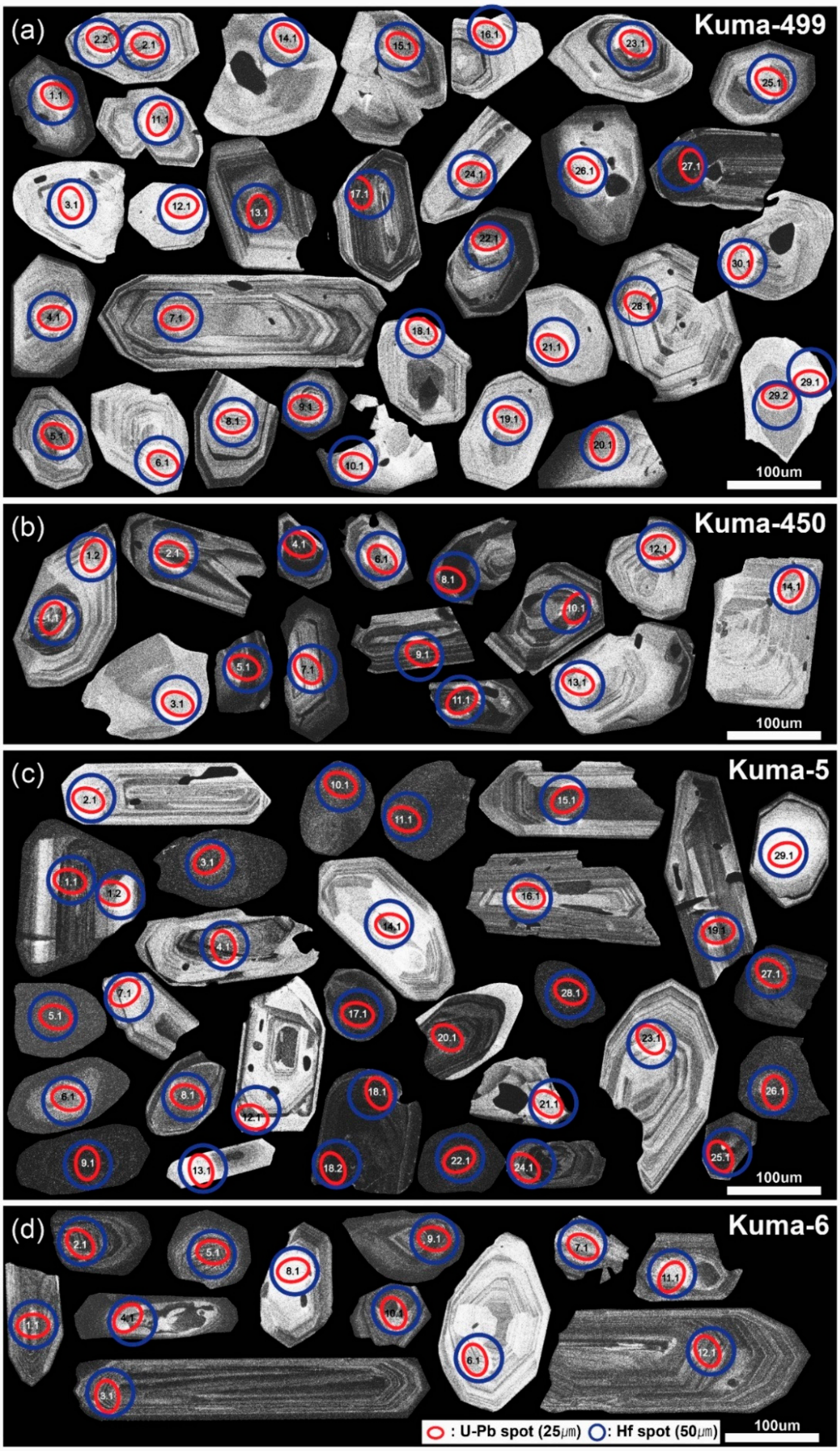

Figure 2. Cathodoluminescence images of studied zircons from the Goshoura and Himenoura Groups. The red and blue ellipses represent U-Pb analysis and Hf analysis spots, respectively. Four samples are shown separately; (**a**) Kuma-449, (**b**) Kuma-450, (**c**) Kuma-5, and (**d**) Kuma-6. The size of spots for Hf isotope analysis (blue) is larger than spots in U-Pb analysis (red). Only the zircon grains of Kuma-5 contain ages older than Cretaceous and those with more developed roundness than other samples.

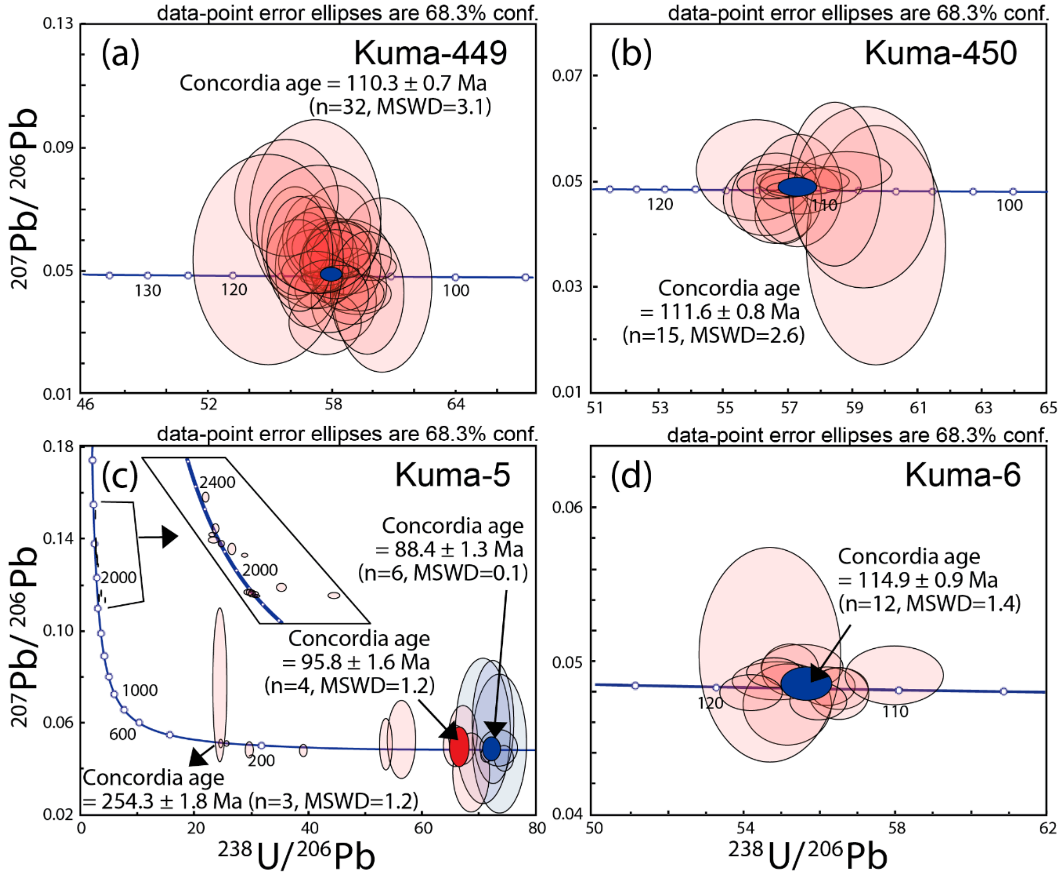

Figure 3. Tera-Wasserburg diagrams of SHRIMP U-Pb detrital zircon ages from the (**a**,**b**) Goshoura Group and (**c**,**d**) Himenoura Group.

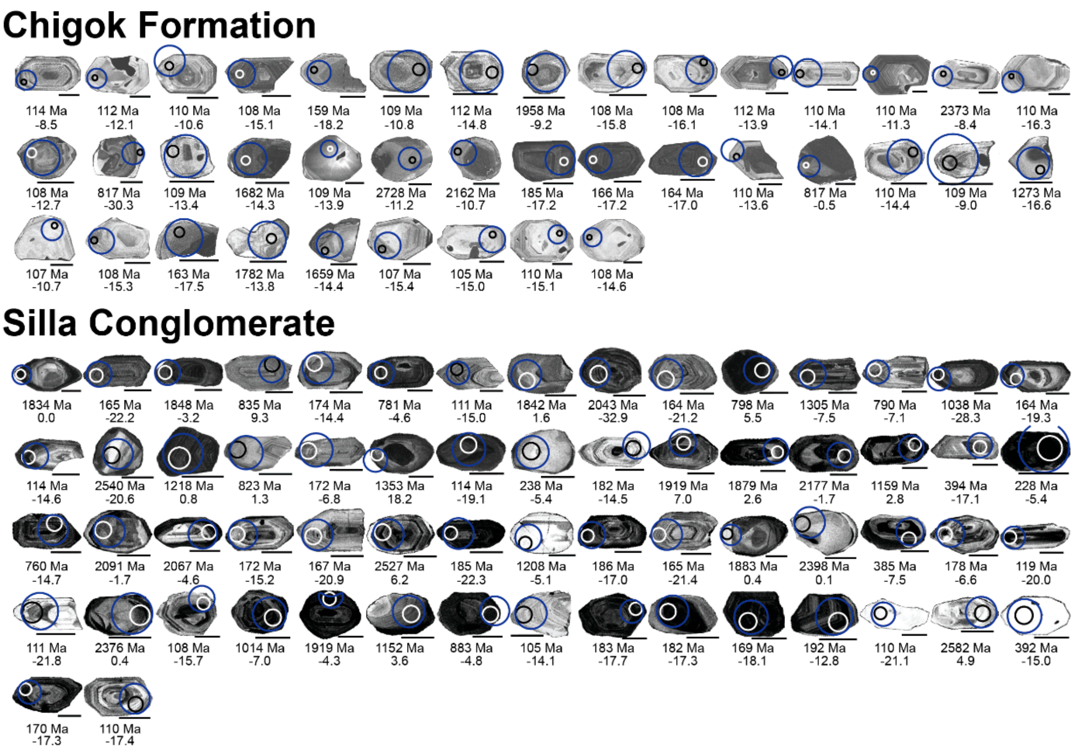

Figure 4. *Cont.*

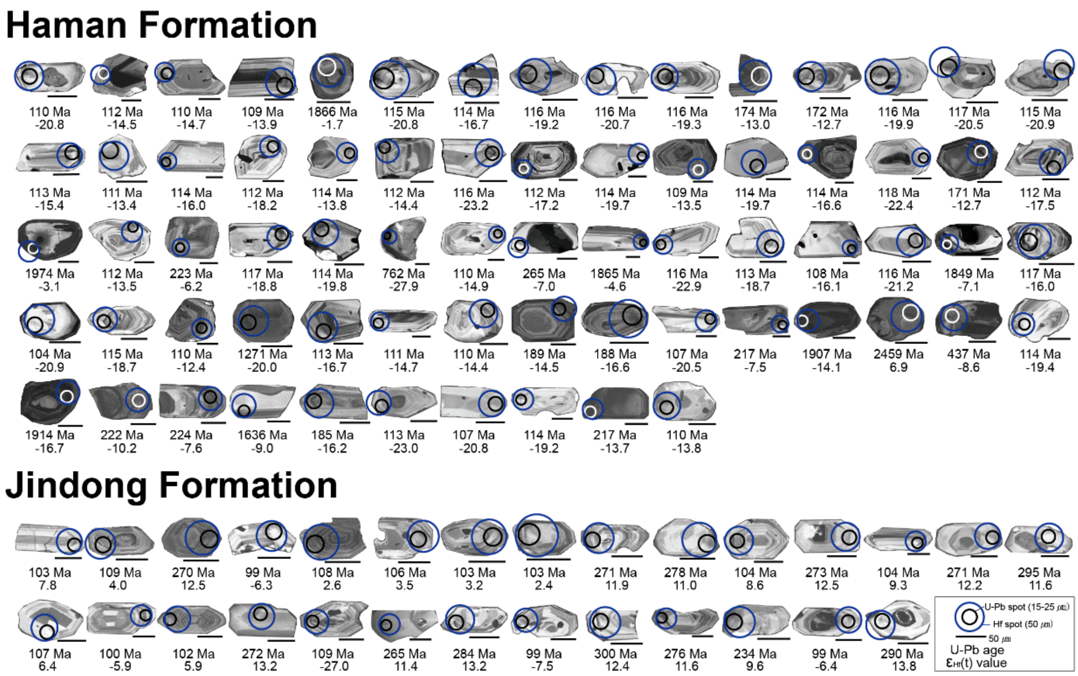

Figure 4. Cathodoluminescence images of studied zircons from the Hayang Group. The small ellipses are the spots for the previous U-Pb age analysis, and the large ellipses are the spots for the Hf analysis.

3.2. Hf Isotopic Compositions of the Detrital Zircons from the Goshoura and Himenoura Groups, SW Japan

The analyzed Hf isotope compositions of the detrital zircons from the Goshoura Group and Himenoura Group in SW Japan are listed in Table A2. Of the four samples from the Goshoura Group and Himenoura Group, three with similar concordia ages of about 110–115 Ma exhibit positive $\varepsilon_{Hf}(t)$ values of +8.5 to +3.6 except for one analysis spot (Kuma-450-3.1) with a value of -7.8 (Figure 5). Their T_{2DM} age ranges from 842 Ma to 560 Ma, and the exceptional spot (Kuma-450-3.1) has an older T_{2DM} age of 1469 Ma. Sample Kuma-5, however, shows a wide range of $\varepsilon_{Hf}(t)$ values (+9.3 to −21.1) and T_{2DM} ages (580 Ma to 2805 Ma). Among them, the $\varepsilon_{Hf}(t)$ values of the Cretaceous zircons are divided into two groups: +8.2 to +0.1 and −14.7 to −21.1. Jurassic zircon of Kuma-5 has an $\varepsilon_{Hf}(t)$ value of −19.6 and a T_{2DM} age of 2163 Ma. From late Permian to Triassic, zircons have $\varepsilon_{Hf}(t)$ from +9.3 to +2.6, and Precambrian zircons range from +3.4 to −3.3.

3.3. Hf Isotopic Compositions of the Detrital Zircons from the Hayang Group, Korea

In this study, Hf isotope composition was also analyzed from detrital zircons of Hayang Group in Gyeongsang basin, Korea (Table A3), which had already analyzed U-Pb ages [19]. The detrital zircons of the Hayang Group have a much wider range of U-Pb ages [19] than those of the Goshoura and Himenoura groups. The $\varepsilon_{Hf}(t)$ values of detrital zircons of the Hayang Group show significant changes with geological age. The Cretaceous detrital zircon grains mostly preserve the euhedral shape with sharp crystal edges, but the older zircon grains tend to develop roundness (Figure 4). In the case of Cretaceous zircons, which are almost half of all zircons, the $\varepsilon_{Hf}(t)$ value varies from −27.0 to +9.3 (Figure 5). Interestingly, negative $\varepsilon_{Hf}(t)$ values appear in all the lower three formations of the Hayang Group, and positive values appear only in the Jindong Formation at the top. The $\varepsilon_{Hf}(t)$ of the Jurassic and Triassic zircons ranges from −22.3 to −5.4. In the Jindong Formation, unlike other formations, a large number of Permian zircons appear and have fairly high positive $\varepsilon_{Hf}(t)$ values from +11.0 to +13.8. The Paleoproterozoic and Archean zircons of the Hayang Group show $\varepsilon_{Hf}(t)$ values of −32.9 to +7.0 (Figure 5). The Neoproterozoic and Mesoproterozoic zircons of the Hayang Group have a significant range of the $\varepsilon_{Hf}(t)$ values from −30.3 to +18.2.

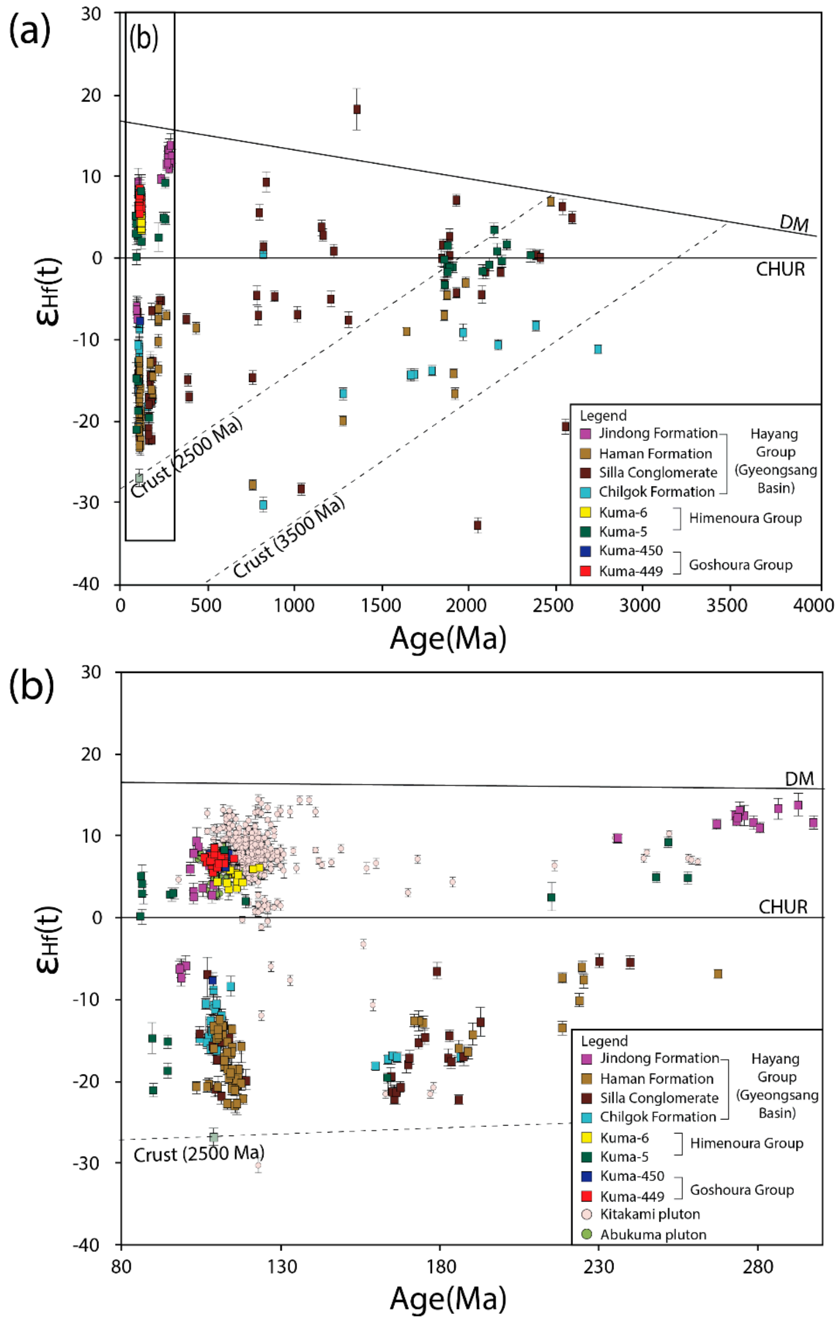

Figure 5. Plot of zircon $\varepsilon_{Hf}(t)$ versus crystallization ages. The evolutionary path of the depleted mantle is based on $^{176}Lu/^{177}Hf$ and $^{176}Hf/^{177}Hf$ ratios from Griffin et al. [48]. The evolution lines for the continental crust with ages of 2500 Ma and 3500 Ma were drawn using the Lu/Hf ratio (=0.081) of Rudnick and Gao [49]. (**a**) Plot of zircon $\varepsilon_{Hf}(t)$ versus crystallization ages for the entire age range. (**b**) A plot expanded only in the range of about 80–300 Ma.

4. Discussion

4.1. Provenance of Detrital Zircons of the Goshoura and Himenoura Groups

The detrital zircon grains of the three of the four samples from the Goshoura and Himenoura groups (Kuma-499, Kuma-450, and Kuma-6) show euhedral to subhedral shapes with well-preserved crystal edges instead of showing well developed roundness indicating the relatively short sediment transport distance (Figure 2). These samples yield single concordia ages with small errors of 110.3 ± 0.7 Ma, 116.8 ± 0.8 Ma, and 114.9 ± 0.9 Ma, respectively. The Th/U ratios of these zircons (0.25–0.96) are larger than 0.1, which is a general criterion that distinguishes igneous zircons from metamorphic zircons [50]. Therefore, it is presumed that these relatively homogeneous detrital zircons originate from igneous protoliths not far away. In contrast to these, the detrital zircon grains separated from the upper Amura Formation (Kuma-5) of the Himenoura group show a wide range of age distributions and the degree of development of roundness of grains. Among the zircon grains of the sample Kuma-5, Cretaceous ones have euhedral shapes like other samples. However, the older zircon grains show relatively rounded edges. In particular, the Paleoproterozoic zircon grains have more developed roundness (Figure 2c). Although the roundness of detrital zircon grains is not a definite quantitative measure of transport distance, it appears to reflect the degree of age variance and relative transport distance in the analyzed samples. All the analyzed zircons from Kima-5 have Th/U ratios greater than 0.1, implying igneous origin. The youngest concordia ages in the Goshoura Group and the Himenoura Group are 110.3 ± 0.7 Ma and 88.4 ± 1.3 Ma, respectively, somewhat older than previously reported fossil ages [26–29]. Recently, a slightly younger age of 81.5 ± 1.4 Ma was reported from the upper part of the Amura Formation and was suggested as the maximum depositional age [25]. Thus, these Cretaceous zircons were reworked from existing rocks or sediments and are not the product of syn-sedimentary volcanic activity. Among the detrital zircons of sample Kuma-5, the proportion of Paleoproterozoic is about 45%.

The U-Pb concordant ages calculated from detrital zircons of the Goshoura Group and Himenoura Group were 114.9 ± 0.9 Ma, 111.6 ± 0.8 Ma, 110.3 ± 0.7 Ma, 95.8 ± 1.6 Ma, and 88.4 ± 1.3 Ma. The U-Pb ages of the granitoids of the Higo metamorphic belt, the basement rock of Goshoura and Himenoura Groups, were reported from ca. 117 Ma to 108 Ma [51,52]. These Cretaceous ages of the Higo belt are consistent with the detrital zircon ages of the Goshoura and Himenoura groups with concordia ages of about 115 Ma to 110 Ma. Accordingly, the Higo belt is inferred as the main source of the Cretaceous detrital zircons of about 115–110 Ma deposited in Goshoura and Himenoura Groups. However, the U-Pb age of Amura Formation (Kuma-5), the upper layer of the Cretaceous Himenora group, shows ages between 2357 Ma and 86 Ma. More than 45% of these consist of Paleoproterozoic zircons, showing a different age distribution pattern than the other three samples. Although the Paleoproterozoic zircons should have been derived from the old continental crust, rocks of that age have not yet been reported on the Japanese Islands. However, on the Korean peninsula close to Japan, Paleoproterozoic rocks [53,54] corresponding to the zircon ages of Kuma-5 are exposed to the surface in a large area. Given the interconnection of the Korean Peninsula and the Japanese Islands before the opening of the East Sea (Sea of Japan) in Cenozoic [55], the presence of these Paleoproterozoic zircons indicates the supply of sediments from the inland area, presumably the current Korean Peninsula. We suggest that the basin-fills from the middle to the upper-middle part of the Cretaceous Basin in the Amakusa Islands were initially supplied primarily from source rocks in the nearby Higo belt where Cretaceous igneous rocks of similar age are distributed. However, the sediments of the Amura Formation were supplied from sources within the nearby Higo belt as well as from the distant inland areas.

The sample Kuma-5 of the Himenoura Group also yielded a Permian concordant age of 254.3 ± 1.8 Ma. In fact, Permian igneous rocks have been found in several areas of Japan, including the nearby Kyushu area. The Usukigawa granodiorite, located in east central Kyushu, has a zircon U-Pb age of ca. 290 Ma [52]. The Kinshozan Quartz Diorite from the Kanto Mountains, Japan, has a zircon U-Pb age of 281.5 ± 1.8 Ma [56]. Permian zircon U-Pb ages of 292 to 259 Ma have been reported from granitoids in the Maizuru area [57]. A new U–Pb zircon geochronological study for the paragneisses from the Tateyama area in the Hida Mountains of north central Japan showed that the detrital zircons had a core age of about 275 Ma and overgrowth ages due to metamorphism of around 235–250 Ma [58]. However, in the case of the Himenoura Group, considering that Th/U ratios of all zircons are greater than 0.1 implying igneous origin, it is suggested that Permian igneous rocks from other regions than the paragneiss of the Hida Mountains were the source of the studied detrital zircons.

Hf isotopic compositions of the detrital zircons are also helpful in tracking the provenance of sediments. The $\varepsilon_{Hf}(t)$ values of the Jurassic and Triassic zircons of the Hayang Group ranges from −18.2 to −5.4 and agree well with typical values for Jurassic and Triassic granitoids known in South

Korea [59,60]. The Paleoproterozoic and Archean zircons of the Hayang Group have $\varepsilon_{Hf}(t)$ values of −14.8 to +6.9 and are similar to the Paleoproterozoic basement rocks of the Yeongnam massif surrounding the Gyeongsang basin [54,61]. The Neoproterozoic and Mesoproterozoic zircons of the Hayang Group appear to have been derived from the Okcheon metamorphic belt in the northwest [19]. During this period, the $\varepsilon_{Hf}(t)$ values of zircons show a significant range of changes from −30.3 to +18.2. The lower values appear to follow the evolution curve of the Archean continental crust, like the Paleoproterozoic and Archean zircons (Figure 5). However, some higher values seem to reflect the input of juvenile material from the depleted mantle at the time. This is consistent with the high $\varepsilon_{Hf}(t)$ values reported from constituent members of the Okcheon metamorphic belt, reflecting rifting events related to breakup in supercontinent Columbia during the Mesoproterozoic [62].

4.2. Resumption of Igneous Activities at about 120 Ma after a Break for 40 Ma

In the Korean peninsula and Japanese islands located at the eastern margin of the Eurasia continent, there was a long resting period without active magmatism from about 160 Ma to about 120 Ma [16–18]. Therefore, in the detrital zircons of the Cretaceous basins of these regions, ages during this long magmatic gap are hardly found. In the Nakdong Formation, the lowermost part of the Cretaceous Gyeongsang basin in the southeastern part of the Korean Peninsula, about 128 Ma of igneous zircons were found [11]. This age marks the beginning of the deposition of the Nakdong Formation, that is, the beginning of the development of the Cretaceous Gyeongsan basin. The igneous rock of this age has not yet been discovered in the Korean Peninsula, but granitoids of about 130–110 Ma are widely exposed in the Kitakami zone in Northeast Japan [63,64]. The emergence of granitoid plutons of this age in the Japanese islands indicates the resumption of igneous activity after a similar magmatic gap on the Korean Peninsula.

In the detrital zircons of the Himenoura Group and the Goshoura Group in southwestern Japan and the Hayang Group in the southeastern Korean peninsula, zircons of about 120–110 Ma, which are about 10–20 Ma younger than the Nakdong Formation, are common. Both the Korean peninsula and the Japanese islands, igneous rocks of this range of age are more common than those of about 120–130 Ma. Granitoids of 109–114 Ma are distributed in the southwestern part of North Korea [65]. In the western and central regions of the Gyeonggi massif in South Korea, igneous activities of about 110 Ma have been reported [66]. In Southwest Japan, several plutonic rocks in the central Kyushu region have zircon U-Pb ages of 108–117 Ma: Oshima quartz dioritic gneiss, Oshima granitic gneiss, Ryuhozan gabbro, Miyanohara tonalite, and Mansaka tonalite [51,52]. Zircon U–Pb ages of plutonic rocks in the southern Abukuma Mountains of Northeast Japan indicate that the intrusion ages of gabbroic rocks and surrounding granitic rocks ranges from 113 to 100 Ma [67]. Taken together, it seems that the long paused magmatism has resumed at about 130 Ma in the Kitamami zone in Northeast Japan. However, in a wide area extending to Southwest Japan and the Korean Peninsula, there seems to have been active magmatism at about 120–110 Ma a little later.

4.3. Input of Juvenile Mantle Material with Resumption of Magmatism

The detrital zircon of igneous origin retains the original hafnium isotopic value of the melt from which it was crystallized without post-crystallization radiogenic growth due to the low Lu/Hf ratio. Therefore, the Hf isotope values of detrital zircons are suitable for examining tectonic environment related to magmatism in their provenance [21,68]. The results of this study and the age distribution of Cretaceous granitoids in Korea and Japan show that there was a very active igneous activity from about 130–120 Ma after a magmatic gap of 30–40 Ma beginning at about 160 Ma. The Hf isotope composition in the detrital zircons of this period are characterized bimodal $\varepsilon_{Hf}(t)$ values of quite positive and significant negative values. Among the analysis results, most of the Cretaceous zircons of the Goshoura and Himenoura groups in Japan have positive $\varepsilon_{Hf}(t)$ values, but in the case of the Hayang Group on the Korean Peninsula, on the contrary, the Cretaceous zircons of the other formations except the Jindong Formation show negative values. Among these positive Cretaceous zircons are discussed first, and other results are discussed later.

The Mesozoic granitoids of the SW Japan mostly have $\varepsilon_{Nd}(t)$ values in the range of −15 to +5 and an average value of about −4, which is interpreted to have a source rock containing a large amount of recycled continental crust [69]. However, the Early Cretaceous detrital zircons of the Goshoura and Himenoura groups have a more depleted value of positive $\varepsilon_{Hf}(t)$, so it is necessary to investigate the cause. In general, high $\varepsilon_{Hf}(t)$ values indicate origin from depleted mantle or juvenile young oceanic crust, while low $\varepsilon_{Hf}(t)$ values represent origin from old continental crust sources [70]. Therefore, the positive $\varepsilon_{Hf}(t)$ of the Early Cretaceous zircons of the Goshoura and Himenoura groups represents the input of juvenile materials from the depleted mantle. Meanwhile, Early Cretaceous granitoids in the Kitakami zone in Northeast Japan have positive $\varepsilon_{Hf}(t)$ values [63] that are similar to or slightly higher than the Cretaceous detrital zircons in this study (Figure 5). Early Cretaceous Kitakami granitic plutons have been suggested to include rocks of adakitic affinity and mostly derived from juvenile oceanic crustal sources [64]. The generation model of adakitic magma includes the melting of young oceanic crusts or the melting of eclogite created by underplating these oceanic crusts underneath the crust [71–74]. The melts generated in this way may contain juvenile materials derived from depleted mantle in a high proportion, and thus the $\varepsilon_{Hf}(t)$ value may be quite high [75].

During the early Cretaceous period of 120–110 Ma, numerous igneous rocks were emplaced over large areas of Japan, including, for example, Ryoke-Sanyo batholith and a number of numerous granitoids distributed in the Abukuma belt, Sikoku area, and Higo belt [51,52,63–67]. Particular attention should be paid to the granitoids of Abukuma and Higo belts. These granitoids have zircon U-Pb ages ranging from 118 Ma to 101 Ma and exhibit the geochemical characteristics of adakite formed by slab melting of young oceanic crusts (e.g., Shiraishino adakitic pluton [76]). Recently, Maki et al. [51] conducted U-Pb age determination and Hf isotope analysis of diatexitic migmatite on Higo belts and obtained an age of 110.1 ± 0.6 Ma (n = 11, MSWD = 1.10) and high $\varepsilon_{Hf}(t)$ values up to +11.8. They also argued that the presence of diatexitic migmatite with high $\varepsilon_{Hf}(t)$ values reflects the influence of the highly depleted mantle and juvenile components, and may be related to the remelting of basalt produced from the depleted mantle. Coeval igneous rocks affected by depleted mantle-derived juvenile components have also been reported in Abukuma, in northeastern Japan. Tsuchiya et al. [64] claimed that the Cretaceous Abukuma granite had an age of 118–117 Ma and the geochemical characteristics of adakite. Therefore, the inclusion of juvenile mantle materials in magmatism that resumed after a long resting period was confirmed not only in detrital zircons in sedimentary formations in Southwest Japan, but also in 120–110 Ma granitoids in Northeast Japan.

4.4. Negative $\varepsilon_{Hf}(t)$ Values of Cretaceous Zircons

The $\varepsilon_{Hf}(t)$ values of the Cretaceous detrital zircons analyzed in this study show a bimodal distribution pattern that is divided into a fairly positive group and a significantly negative group. The positive group appears in Himenoura and Goshoura groups and Jindong Formation, and the negative group appears mainly in Chilgok, Silla, and Haman formations (Figure 5). That is, the positive group appears mainly on the Japanese side, and the negative group appears mostly on the Korean side, except for some zircons of Jindong Formation. One thing to note here is that when Jindong Formation was deposited, the flow direction of paleocurrent indicates the supply of sediment from the east, or the Japanese side [32,37–39]. Therefore, the detrital zircons of the positive group appearing in Jindong Formation may originate from sediment sources in Japan. Considering this, it suggests that the igneous activities at that time had the characteristics of mainly positive $\varepsilon_{Hf}(t)$ in the vicinity of the trench and significantly negative $\varepsilon_{Hf}(t)$ in the inland side. The fairly low $\varepsilon_{Hf}(t)$ values in the inland indicate that magma genesis and differentiation processes were affected by old crustal materials below the Korean Peninsula. A similar range of negative $\varepsilon_{Hf}(t)$ values can be seen in the Triassic to Jurassic igneous rocks of the Korean Peninsula [60]. This characteristic also appears in the $\varepsilon_{Hf}(t)$ values of the Triassic to Jurassic detrital zircons (−5 to −25) included in sedimentary layers of the Hayang Group (Figure 5) reflecting the influence of materials from the old continental curst of the Korean Peninsula.

4.5. Variability of $\varepsilon_{Hf}(t)$ Values Over Time

The high ε_{Hf}(t) values of about 120–110 Ma detrital zircons are somewhat different from those previously reported from the Cretaceous to Paleogene granitoids from Southwest Japan. For example, the granitic rocks in the Iwakuni area in Southwest Japan have a zircon U-Pb age of 104–92 Ma and ε_{Hf}(t) in the range of −5 to +0.7 [77]. The results of Sr-Nd isotope analysis for Phanerozoic granitoids from Southwest Japan generally show negative ε_{Nd}(t) values and high initial $^{87}Sr/^{86}Sr$ ratios [69]. Therefore, it is clear that there was a temporal change from the high ε_{Hf}(t) values of Early Cretaceous to the lower values of the later period. When ridge subduction occurs, the volume of the melting zone may be larger because of the enhanced temperature, and continental materials in the lower crust may be added to the melt. The magma formed in the later stages through this process may have a larger proportion of enriched materials compared to the earlier ones mainly derived from the young oceanic crust.

However, the temporal change of isotope values from depleted values to more enriched values does not appear only in the Cretaceous period. It is known that there was Permian igneous activity in both Korea and Japan, and it seems that there was no magmatism for a long time before that. The Permian zircons (270–300 Ma) of the Jindong Formation, which originated in Japan, show that the ε_{Hf}(t) values of Permian granitoids appearing after the dormant period of magmatism are quite high, ranging from +11 to +14 (Figure 5). The Yeongdeok granite, located in the east-central part of the Korean peninsula at about 260 Ma, slightly younger than the Permian zircons of the Jindong Formation, also has adakitic characteristics and at the same time has an ε_{Hf}(t) value of about +11.5, depleted isotopic composition [60]. In the Hayang Group, the ε_{Hf}(t) values of Triassic to Jurassic detrital zircons also show a shift toward more enriched isotope composition than those of Permian (Figure 5). The tectonics of repetitive changes in the ε_{Hf}(t) values in the Pacific type of orogenic cycle are outside the scope of this study, but it is worth noting.

4.6. Since Early Cretaceous, Japanese Islands Have Moved 1000 km Northeast from Next to South China?

Researchers of the Kitakami adakites argue that the magmatism of the time was caused by ridge subduction that migrated northward, and that these plutons were translated northeastward more than 1000 km from their original location next to South China [5]. However, considering the relationship with neighboring blocks, such a long-distance movement is not very persuasive and seems not necessary. First of all, there seems to be no significant difference in the history of tectonic evolution between Northeast Japan and Southwest Japan. One of the characteristics of Northeast Japan is the existence of Early Paleozoic plutons, which are about 500–450 Ma [12,56]. However, evidence of igneous activity in the Paleozoic era corresponding to this period was also found in Southwest Japan. The LA-ICP-MS zircon U–Pb geochronology revealed that the intrusion age of Saganoseki quartz diorite was 473.3 ± 3.6 Ma [78].

Early Cretaceous tectonic environments also appear to be similar in Northeast and Southwest Japan. The resumption of subduction-related igneous activity after a long resting period can be determined by the age of about 130–110 Ma granitoids that occur in various parts of Japan and by the age distribution patterns of detrital zircons in sediments. In the case of Northeast Japan, the age of plutons intruded in the Kitakami zone includes those of about 130–120 Ma. In the case of Southwest Japan, the maximum age of Early Cretaceous plutons or detrital zircons is about 120 Ma, suggesting that igneous activity may have begun in Northeast Japan slightly earlier than in Southwest Japan. However, both regions are similar in that the restarted magmatism has a high hafnium initial isotopic composition, indicating the melting of the material derived from the young oceanic crust. Since the resumption of magmatism was almost the same and the properties of the source material were similar, it is highly likely that the two regions shared the same tectonic setting. Several evidences have suggested that Southwest Japan and the Korean Peninsula were connected to each other in the Early Cretaceous period [55]. In particular, the research shows that during the Cretaceous period sediment was supplied from Japan to Korea and from Korea to Japan, depending on the location, supporting this [19,22,23,79]. This connection between Southwest Japan and the Korean Peninsula in

Early Cretaceous contradicts the suggestion that Northeast Japan or the whole of Japan is located next to south China in Early Cretaceous and moved about 1000 km northeast to its present location.

5. Conclusions

Most of the detrital zircons of the Goshoura and Himenoura groups in west central Kyushu in Southwest Japan have U-Pb ages in the Cretaceous period, but some have older Permian or Paleoproterozoic ages. The detrital zircons with Paleoproterozoic ages indicate sediment supply from the inland area, possibly from the Korean Peninsula that was connected during their deposition. The Cretaceous age of about 120–110 Ma indicates that magmatism resumed after the previous dormant period, and the Japanese zircons have quite positive ε_{Hf}(t) values. These detrital zircons, which appear to have originated from the igneous rocks of Southwest Japan, are likely to have been produced by ridge subduction that led to the melting of the young oceanic crust. We suggested that later Japanese granitoids generally show a more enriched isotope composition as a result of the melting of a wider volume as the ridge subduction proceeds and contain more crust components. All of the Cretaceous zircons of the Hayang Group have quite negative ε_{Hf}(t) values, except for the Jindong Formation, which had a sediment supply from Japan. This is interpreted as the fact that the old continental crust material on the Korean Peninsula was included in the magma generation. The subduction-related magmatism started in Permian shows the characteristics of adakite generation and high ε_{Hf}(t) value. Meanwhile, the composition of subsequent magmatisms changed to more enriched. This repetitive trend of change can be a typical example of the Pacific-type orogenic cycle.

Author Contributions: Conceptualization, T.-H.L. and K.-H.P.; methodology, K.-H.P.; validation, T.-H.L. and K.-H.P.; formal analysis, T.-H.L.; investigation, K.-H.P.; writing—original draft preparation, K.-H.P.; writing—review and editing, K.-H.P.; visualization, T.-H.L.; supervision, K.-H.P.; funding acquisition, K.-H.P. All authors have read and agreed to the published version of the manuscript.

Funding: This work was supported by the National Research Foundation of Korea (NRF) grant funded by the Korea government (MSIT) (No. NRF-2019R1A2C2002506). This research was also supported by a grant (GP2020-014) from the Research in Active Tectonics and Development of Fault Segmentation Model for Intraplate regions from Basic Research Project of the Korea Institute of Geoscience and Mineral Resources (KIGAM) funded by the Korean Ministry of Science and ICT.

Acknowledgments: We would like to thank Komatsu who organized and guided fourth international symposium and field trip of the IGCP507. We deeply appreciate the meticulous and constructive opinions of the anonymous reviewers.

Conflicts of Interest: The authors declare no conflict of interest. The funders had no role in the design of the study; in the collection, analyses, or interpretation of data; in the writing of the manuscript, or in the decision to publish the results.

Appendix A

Table A1. SHRIMP U-Pb results for the detrital zircons from the Goshoura and Himenoura Groups, Southwest Japan.

Spot No.	U (ppm)	Th (ppm)	Th/U	Common ^{206}Pb (%)	^{238}U/^{206}Pb	± (%)	^{207}Pb/^{206}Pb	± (%)	Apparent Age (Ma)
					Kuma-449				
Kuma-449-1.1	224	103	0.48	0.00	57.0	1.6	0.0611	14.8	110.3 ± 1.3
Kuma-449-2.1	247	118	0.50	0.06	58.6	1.8	0.0412	20.5	110.1 ± 1.6
Kuma-449-2.2	234	111	0.49	0.37	58.2	1.8	0.0662	11.8	107.3 ± 1.7
Kuma-449-3.1	105	69	0.68	0.00	60.4	2.7	0.0461	39.9	106.1 ± 1.5
Kuma-449-4.1	321	212	0.68	0.20	58.0	2.2	0.0580	11.0	108.9 ± 2.2
Kuma-449-5.1	596	262	0.45	0.00	59.2	1.8	0.0431	9.9	108.6 ± 1.9
Kuma-449-6.1	208	98	0.49	0.00	58.7	2.4	0.0552	14.4	107.9 ± 2.4
Kuma-449-7.1	508	211	0.43	0.09	60.0	1.3	0.0519	5.6	106.1 ± 1.3
Kuma-449-8.1	289	128	0.46	0.00	57.7	2.0	0.0341	19.7	112.8 ± 2.1
Kuma-449-9.1	429	248	0.60	0.00	57.2	1.1	0.0447	8.9	112.3 ± 1.1
Kuma-449-10.1	206	85	0.43	0.56	59.0	1.9	0.0457	17.8	108.7 ± 1.8
Kuma-449-11.1	219	145	0.68	0.00	58.0	1.5	0.0536	16.6	109.5 ± 1.2
Kuma-449-12.1	122	53	0.45	0.03	56.2	1.9	0.0597	19.8	112.0 ± 1.4
Kuma-449-13.1	1006	533	0.55	0.07	57.9	0.9	0.0480	5.3	110.5 ± 1.0
Kuma-449-14.1	265	95	0.37	0.00	57.2	2.1	0.0537	12.7	110.9 ± 2.1
Kuma-449-15.1	428	202	0.49	0.00	59.3	1.3	0.0435	8.6	108.3 ± 1.4
Kuma-449-16.1	198	148	0.77	0.00	58.7	1.9	0.0524	17.9	108.4 ± 1.7
Kuma-449-17.1	1059	751	0.73	0.00	57.6	1.2	0.0482	3.0	111.0 ± 1.3
Kuma-449-18.1	203	94	0.48	5.23	56.8	1.8	0.0511	23.7	112.1 ± 1.2
Kuma-449-19.1	242	123	0.53	0.28	57.4	1.9	0.0597	12.7	109.7 ± 1.8
Kuma-449-20.1	327	216	0.68	0.00	58.3	1.8	0.0580	9.5	108.2 ± 1.8
Kuma-449-21.1	100	58	0.60	0.00	57.2	3.7	0.0688	29.1	108.9 ± 3.0
Kuma-449-22.1	378	203	0.56	0.37	57.2	1.9	0.0503	8.7	111.4 ± 2.0
Kuma-449-23.1	227	113	0.51	0.07	56.3	1.8	0.0550	14.7	112.5 ± 1.7
Kuma-449-24.1	226	151	0.69	0.02	58.2	1.9	0.0529	13.8	109.3 ± 1.9
Kuma-449-25.1	178	97	0.56	0.00	59.7	2.0	0.0437	29.7	107.7 ± 1.3
Kuma-449-26.1	133	71	0.55	0.00	55.8	3.0	0.0741	16.7	110.8 ± 2.8
Kuma-449-27.1	1754	839	0.49	0.32	58.4	1.0	0.0503	2.8	109.1 ± 1.1
Kuma-449-28.1	306	197	0.67	0.00	57.8	2.2	0.0426	18.0	111.3 ± 2.3
Kuma-449-29.1	82	40	0.50	0.00	54.9	4.4	0.0543	41.0	115.5 ± 3.9
Kuma-449-29.2	150	115	0.79	0.07	56.4	1.9	0.0562	21.7	112.1 ± 1.5
Kuma-449-30.1	160	79	0.51	0.13	57.4	3.5	0.0641	21.2	109.2 ± 3.4

Table A1. *Cont.*

Spot No.	U (ppm)	Th (ppm)	Th/U	Common ^{206}Pb (%)	^{238}U/^{206}Pb	± (%)	^{207}Pb/^{206}Pb	± (%)	Apparent Age (Ma)
				Kuma-450					
Kuma-450-1.1	539	308	0.59	0.07	56.8	1.0	0.0436	7.8	113.1 ± 1.1
Kuma-450-1.2	210	103	0.51	0.00	56.0	2.2	0.0523	12.0	113.5 ± 2.3
Kuma-450-2.1	563	364	0.67	0.00	57.4	1.4	0.0489	6.5	111.3 ± 1.6
Kuma-450-3.1	134	101	0.78	0.00	59.7	2.4	0.0383	38.8	108.4 ± 1.7
Kuma-450-4.1	1072	652	0.63	0.09	56.9	0.9	0.0494	3.1	112.1 ± 1.0
Kuma-450-5.1	907	398	0.45	0.30	57.5	1.6	0.0503	3.4	110.9 ± 1.8
Kuma-450-6.1	324	178	0.57	0.17	56.3	1.5	0.0467	9.4	113.8 ± 1.6
Kuma-450-7.1	263	196	0.77	0.00	56.6	1.6	0.0471	11.9	113.0 ± 1.7
Kuma-450-8.1	2321	1247	0.55	0.32	57.1	0.9	0.0488	1.8	111.9 ± 0.9
Kuma-450-9.1	871	528	0.63	0.02	56.5	1.3	0.0497	3.7	112.9 ± 1.4
Kuma-450-10.1	862	509	0.61	0.20	58.8	1.6	0.0522	4.6	108.1 ± 1.7
Kuma-450-11.1	1027	817	0.82	0.00	58.3	1.1	0.0495	4.8	109.5 ± 1.2
Kuma-450-12.1	237	130	0.57	0.17	57.3	1.6	0.0485	14.4	111.5 ± 1.5
Kuma-450-13.1	145	89	0.63	0.00	59.3	2.4	0.0472	23.8	107.9 ± 2.4
Kuma-450-14.1	155	110	0.73	0.12	58.5	1.6	0.0497	20.5	109.1 ± 1.2
				Kuma-5					
Kuma-5-1.1	706	413	0.60	1.34	2.9	0.9	0.1290	0.4	2084.6 ± 6.6
Kuma-5-1.2	94	68	0.75	0.76	2.7	1.3	0.1314	1.1	2116.6 ± 19.0
Kuma-5-2.1	128	59	0.48	0.00	73.8	4.3	0.0520	38.1	86.3 ± 3.1
Kuma-5-3.1	287	159	0.57	0.06	2.5	1.0	0.1334	0.6	2142.9 ± 10.2
Kuma-5-4.1	759	333	0.45	0.04	66.7	1.0	0.0511	7.0	95.6 ± 0.9
Kuma-5-5.1	325	33	0.10	0.00	2.9	1.6	0.1151	0.6	1882.2 ± 11.3
Kuma-5-6.1	142	104	0.75	0.22	2.5	1.2	0.1391	0.9	2216.1 ± 14.8
Kuma-5-7.1	416	149	0.37	0.00	66.0	2.1	0.0511	11.6	96.5 ± 1.9
Kuma-5-8.1	324	87	0.28	0.09	3.0	1.5	0.1150	0.6	1879.6 ± 11.4
Kuma-5-9.1	1626	1379	0.88	3.90	4.0	1.3	0.1139	0.6	1862.6 ± 11.7
Kuma-5-10.1	453	198	0.45	0.00	2.4	1.1	0.1368	0.4	2186.9 ± 6.5
Kuma-5-11.1	863	150	0.18	0.06	3.0	1.1	0.1138	0.3	1861.7 ± 5.8
Kuma-5-12.1	775	603	0.80	5.07	67.4	2.5	0.0557	15.0	94.0 ± 2.1
Kuma-5-13.1	120	87	0.74	2.66	70.9	4.4	0.0575	35.8	89.2 ± 3.2
Kuma-5-14.1	136	104	0.79	0.00	72.8	3.3	0.0613	28.6	86.5 ± 2.2
Kuma-5-15.1	579	438	0.78	0.00	74.7	1.5	0.0456	7.9	86.0 ± 1.2
Kuma-5-16.1	188	194	1.06	0.00	68.8	3.0	0.0396	28.5	94.0 ± 2.6

Table A1. *Cont.*

Spot No.	U (ppm)	Th (ppm)	Th/U	Common ^{206}Pb (%)	^{238}U/^{206}Pb	± (%)	^{207}Pb/^{206}Pb	± (%)	Apparent Age (Ma)
Kuma-5									
Kuma-5-17.1	657	88	0.14	1.74	3.3	1.3	0.1170	0.8	1910.3 ± 15.2
Kuma-5-18.1	880	258	0.30	0.08	24.5	0.9	0.0520	2.2	257.6 ± 2.4
Kuma-5-18.2	2013	618	0.32	0.32	25.5	1.1	0.0520	1.5	247.6 ± 2.8
Kuma-5-19.1	420	234	0.58	0.26	73.7	3.0	0.0502	10.3	86.7 ± 2.6
Kuma-5-20.1	750	291	0.40	0.11	39.1	1.2	0.0491	3.6	162.9 ± 1.9
Kuma-5-21.1	160	104	0.67	0.00	56.5	2.9	0.0539	20.6	112.3 ± 2.9
Kuma-5-22.1	221	92	0.43	0.00	3.0	1.1	0.1148	0.7	1876.4 ± 13.1
Kuma-5-23.1	209	111	0.55	0.10	53.7	1.4	0.0518	14.1	118.4 ± 1.4
Kuma-5-24.1	558	419	0.78	0.16	29.6	1.6	0.0493	4.7	214.8 ± 3.3
Kuma-5-25.1	1260	1332	1.09	0.11	71.5	0.9	0.0472	4.4	89.6 ± 0.8
Kuma-5-26.1	257	218	0.88	0.00	2.4	1.9	0.1348	0.6	2161.0 ± 9.9
Kuma-5-27.1	116	58	0.51	0.62	2.3	1.2	0.1509	0.8	2356.5 ± 13.9
Kuma-5-28.1	267	50	0.19	0.00	2.9	1.0	0.1152	0.7	1883.4 ± 12.3
Kuma-5-29.1	35	23	0.67	0.17	24.3	3.3	0.0774	28.3	251.2 ± 4.7
Kuma-6									
Kuma-6-1.1	828	342	0.43	0.18	55.4	1.3	0.0511	2.5	114.9 ± 1.5
Kuma-6-2.1	1106	264	0.25	0.02	56.2	0.9	0.0488	1.8	113.7 ± 1.0
Kuma-6-3.1	1049	270	0.27	0.01	56.5	0.9	0.0483	1.9	113.1 ± 1.0
Kuma-6-4.1	614	361	0.61	0.15	55.4	0.9	0.0471	3.5	115.6 ± 1.1
Kuma-6-5.1	1320	333	0.26	0.06	54.9	1.4	0.0478	2.1	116.4 ± 1.7
Kuma-6-6.1	297	144	0.50	0.00	55.3	1.4	0.0441	6.5	116.1 ± 1.6
Kuma-6-7.1	718	176	0.25	0.00	56.7	0.9	0.0454	3.8	113.1 ± 1.1
Kuma-6-8.1	234	94	0.42	0.27	55.5	2.4	0.0390	17.1	116.6 ± 2.7
Kuma-6-9.1	1908	1158	0.63	0.13	54.8	0.9	0.0487	1.5	116.5 ± 1.0
Kuma-6-10.1	1057	981	0.96	0.00	56.0	0.9	0.0475	1.7	114.3 ± 1.0
Kuma-6-11.1	496	159	0.33	0.12	58.2	1.5	0.0460	4.5	110.1 ± 1.6
Kuma-6-12.1	1030	240	0.24	0.00	54.3	1.0	0.0455	2.6	118.0 ± 1.2

Table A2. LA-MC-ICPMS Lu-Yb-Hf isotopic compositions of the detrital zircons from the Goshoura and Himenoura Groups, Southwest Japan.

Spot No.	$^{176}Hf/^{177}Hf$	±2 S.E.	$^{176}Lu/^{177}Hf$	±2 S.E.	$^{176}Yb/^{177}Hf$	±2 S.E.	$\varepsilon_{Hf}(t)$	T_{2DM} (Ma)
				Kuma-449				
Kuma-449-1.1	0.282918	0.000022	0.001003	0.000033	0.02640	0.00110	7.5	618
Kuma-449-2.1	0.282878	0.000021	0.001383	0.000036	0.03727	0.00074	6.1	699
Kuma-449-2.2	0.282912	0.000019	0.000543	0.000005	0.01354	0.00023	7.3	629
Kuma-449-3.1	0.282913	0.000022	0.000884	0.000015	0.02776	0.00047	7.3	629
Kuma-449-4.1	0.282890	0.000020	0.000919	0.000015	0.02678	0.00058	6.5	674
Kuma-449-5.1	0.282878	0.000023	0.000834	0.000008	0.02204	0.00023	6.1	697
Kuma-449-6.1	0.282919	0.000023	0.000499	0.000007	0.01213	0.00029	7.5	615
Kuma-449-7.1	0.282921	0.000029	0.001699	0.000074	0.05080	0.00230	7.5	616
Kuma-449-8.1	0.282878	0.000024	0.001311	0.000040	0.03700	0.00094	6.1	698
Kuma-449-9.1	0.282889	0.000019	0.000744	0.000008	0.01927	0.00011	6.5	674
Kuma-449-10.1	0.282896	0.000019	0.000592	0.000005	0.01642	0.00017	6.7	661
Kuma-449-11.1	0.282924	0.000021	0.000760	0.000005	0.02049	0.00031	7.7	605
Kuma-449-12.1	0.282889	0.000021	0.000788	0.000023	0.02079	0.00046	6.5	674
Kuma-449-13.1	0.282896	0.000028	0.001848	0.000047	0.05260	0.00150	6.7	665
Kuma-449-14.1	0.282906	0.000025	0.001102	0.000019	0.02969	0.00089	7.1	642
Kuma-449-15.1	0.282888	0.000021	0.000961	0.000010	0.02568	0.00023	6.4	678
Kuma-449-16.1	0.282911	0.000026	0.000928	0.000020	0.02458	0.00041	7.2	632
Kuma-449-17.1	0.282901	0.000027	0.002026	0.000022	0.05705	0.00062	6.8	656
Kuma-449-18.1	0.282914	0.000019	0.000597	0.000015	0.01656	0.00047	7.4	624
Kuma-449-19.1	0.282913	0.000020	0.000736	0.000014	0.01906	0.00053	7.3	627
Kuma-449-20.1	0.282897	0.000025	0.000753	0.000007	0.02042	0.00030	6.7	660
Kuma-449-21.1	0.282857	0.000021	0.000169	0.000005	0.00458	0.00017	5.4	736
Kuma-449-22.1	0.282910	0.000020	0.000775	0.000006	0.02043	0.00028	7.3	633
Kuma-449-23.1	0.282902	0.000024	0.001436	0.000021	0.03838	0.00042	7.0	651
Kuma-449-24.1	0.282918	0.000026	0.000934	0.000033	0.02636	0.00083	7.5	618
Kuma-449-25.1	0.282903	0.000021	0.000809	0.000011	0.02131	0.00020	6.9	648
Kuma-449-26.1	0.282908	0.000020	0.000830	0.000011	0.02521	0.00023	7.2	637
Kuma-449-27.1	0.282926	0.000024	0.001610	0.000021	0.04351	0.00015	7.7	605
Kuma-449-28.1	0.282918	0.000020	0.000842	0.000004	0.02191	0.00031	7.5	617
Kuma-449-29.1	0.282906	0.000027	0.000618	0.000004	0.01617	0.00030	7.2	638
Kuma-449-29.2	0.282931	0.000022	0.000717	0.000016	0.02156	0.00065	8.0	590
Kuma-449-30.1	0.282947	0.000021	0.000721	0.000006	0.01815	0.00030	8.5	560

Table A2. *Cont.*

Spot No.	$^{176}Hf/^{177}Hf$	±2 S.E.	$^{176}Lu/^{177}Hf$	±2 S.E.	$^{176}Yb/^{177}Hf$	±2 S.E.	$\varepsilon_{Hf}(t)$	T_{2DM} (Ma)
Kuma-450								
Kuma-450-1.1	0.282928	0.000024	0.001519	0.000011	0.04262	0.00073	7.9	599
Kuma-450-1.2	0.282913	0.000023	0.000787	0.000021	0.02178	0.00053	7.4	626
Kuma-450-2.1	0.282903	0.000025	0.001422	0.000034	0.04100	0.00130	7.0	649
Kuma-450-3.1	0.282487	0.000028	0.000904	0.000028	0.02606	0.00030	−7.8	1469
Kuma-450-4.1	0.282930	0.000033	0.002822	0.000020	0.08340	0.00160	7.8	601
Kuma-450-5.1	0.282888	0.000027	0.001672	0.000042	0.04930	0.00031	6.4	680
Kuma-450-6.1	0.282926	0.000024	0.001252	0.000027	0.03394	0.00069	7.8	602
Kuma-450-7.1	0.282879	0.000022	0.001085	0.000012	0.03156	0.00036	6.2	695
Kuma-450-8.1	0.282899	0.000028	0.001635	0.000027	0.04670	0.00140	6.8	658
Kuma-450-9.1	0.282917	0.000028	0.001698	0.000061	0.04390	0.00140	7.5	622
Kuma-450-10.1	0.282933	0.000027	0.001956	0.000014	0.05654	0.00044	7.9	593
Kuma-450-11.1	0.282911	0.000030	0.002769	0.000020	0.08077	0.00089	7.1	640
Kuma-450-12.1	0.282920	0.000026	0.001187	0.000019	0.03174	0.00025	7.6	615
Kuma-450-13.1	0.282927	0.000022	0.000652	0.000010	0.01942	0.00050	7.8	600
Kuma-450-14.1	0.282923	0.000022	0.000872	0.000001	0.02547	0.00028	7.7	608
Kuma-5								
Kuma-5-1.1	0.281436	0.000024	0.000698	0.000017	0.02189	0.00065	−1.7	2697
Kuma-5-1.2	0.281440	0.000022	0.000649	0.000012	0.02075	0.00043	−0.8	2673
Kuma-5-2.1	0.282724	0.000027	0.001143	0.000025	0.03455	0.00051	0.1	1012
Kuma-5-3.1	0.281556	0.000026	0.000996	0.000033	0.02516	0.00058	3.4	2467
Kuma-5-4.1	0.282795	0.000023	0.001217	0.000029	0.03730	0.00100	2.8	868
Kuma-5-5.1	0.281583	0.000021	0.000697	0.000040	0.02270	0.00120	−1.0	2498
Kuma-5-6.1	0.281440	0.000019	0.000553	0.000008	0.01506	0.00024	1.6	2624
Kuma-5-7.1	0.282797	0.000020	0.000611	0.000006	0.01812	0.00021	3.0	862
Kuma-5-8.1	0.281578	0.000021	0.001137	0.000013	0.03643	0.00078	−1.8	2539
Kuma-5-9.1	0.281642	0.000028	0.001368	0.000054	0.04480	0.00260	−0.2	2438
Kuma-5-10.1	0.281410	0.000022	0.000740	0.000010	0.02330	0.00038	−0.4	2708
Kuma-5-11.1	0.281515	0.000019	0.000290	0.000025	0.00932	0.00079	−3.3	2609
Kuma-5-12.1	0.282288	0.000025	0.001109	0.000011	0.03300	0.00046	−15.1	1865
Kuma-5-13.1	0.282302	0.000052	0.001120	0.000012	0.03082	0.00040	−14.7	1839
Kuma-5-14.1	0.282839	0.000040	0.001560	0.000039	0.04900	0.00210	4.2	786
Kuma-5-15.1	0.282867	0.000037	0.002031	0.000036	0.06170	0.00160	5.1	732

Table A2. *Cont.*

Spot No.	$^{176}Hf/^{177}Hf$	±2 S.E.	$^{176}Lu/^{177}Hf$	±2 S.E.	$^{176}Yb/^{177}Hf$	±2 S.E.	$\varepsilon_{Hf}(t)$	T_{2DM} (Ma)
				Kuma-5				
Kuma-5-16.1	0.282188	0.000026	0.001402	0.000018	0.04495	0.00062	−18.7	2060
Kuma-5-17.1	0.281558	0.000019	0.000571	0.000031	0.01739	0.00087	−1.1	2526
Kuma-5-18.1	0.282753	0.000022	0.000810	0.000008	0.02376	0.00043	4.8	885
Kuma-5-18.2	0.282762	0.000019	0.001116	0.000006	0.03152	0.00024	4.9	874
Kuma-5-19.1	0.282806	0.000035	0.002902	0.000079	0.08720	0.00210	2.9	855
Kuma-5-20.1	0.282119	0.000018	0.000406	0.000006	0.01236	0.00018	−19.6	2163
Kuma-5-21.1	0.282936	0.000027	0.000690	0.000009	0.01898	0.00030	8.2	580
Kuma-5-22.1	0.281661	0.000021	0.000782	0.000004	0.02435	0.00032	1.5	2357
Kuma-5-23.1	0.282758	0.000025	0.001157	0.000009	0.03000	0.00047	2.0	932
Kuma-5-24.1	0.282717	0.000051	0.001373	0.000017	0.03814	0.00062	2.6	977
Kuma-5-25.1	0.282123	0.000023	0.001819	0.000022	0.05750	0.00100	−21.1	2189
Kuma-5-26.1	0.281481	0.000025	0.001202	0.000023	0.03930	0.00130	0.9	2620
Kuma-5-27.1	0.281312	0.000024	0.000494	0.000006	0.01527	0.00019	0.3	2805
Kuma-5-28.1	0.281574	0.000018	0.000631	0.000038	0.02210	0.00150	−1.2	2510
Kuma-5-29.1	0.282880	0.000020	0.000379	0.000003	0.01141	0.00010	9.3	632
				Kuma-6				
Kuma-6-1.1	0.282858	0.000028	0.002420	0.000110	0.07740	0.00410	5.4	741
Kuma-6-2.1	0.282806	0.000027	0.001689	0.000013	0.04967	0.00057	3.6	842
Kuma-6-3.1	0.282826	0.000026	0.001215	0.000020	0.03730	0.00120	4.3	800
Kuma-6-4.1	0.282855	0.000029	0.001630	0.000053	0.04500	0.00200	5.3	744
Kuma-6-5.1	0.282807	0.000022	0.001164	0.000018	0.03516	0.00063	3.7	836
Kuma-6-6.1	0.282856	0.000030	0.001605	0.000009	0.04725	0.00068	5.4	741
Kuma-6-7.1	0.282876	0.000110	0.001641	0.000076	0.06220	0.00160	6.0	703
Kuma-6-8.1	0.282853	0.000034	0.001212	0.000010	0.03656	0.00079	5.3	746
Kuma-6-9.1	0.282830	0.000027	0.001830	0.000021	0.05562	0.00040	4.5	794
Kuma-6-10.1	0.282871	0.000028	0.001994	0.000068	0.05880	0.00210	5.9	714
Kuma-6-11.1	0.282831	0.000030	0.002176	0.000053	0.06960	0.00170	4.3	795
Kuma-6-12.1	0.282824	0.000023	0.001426	0.000012	0.04204	0.00064	4.3	803

Table A3. LA-MC-ICPMS Lu-Yb-Hf isotopic compositions of the detrital zircons from the Hayang Group, Korea.

Spot No.	$^{176}Hf/^{177}Hf$	±2 s.d.	$^{176}Lu/^{177}Hf$	±2 s.d.	$^{176}Yb/^{177}Hf$	±2 s.d.	Apparent Age (Ma)	$\varepsilon_{Hf}(t)$	T_{2DM} (Ma)
Chilgok Formation									
ChG-1_1.1	0.282462	0.000034	0.000777	0.000032	0.023650	0.000440	114.2	−8.5	1515
ChG-1_2.1	0.282363	0.000021	0.000603	0.000010	0.021250	0.000500	111.5	−12.1	1709
ChG-1_3.1	0.282405	0.000023	0.000552	0.000015	0.016280	0.000230	110.0	−10.6	1628
ChG-1_4.1	0.282281	0.000024	0.001185	0.000013	0.040840	0.000470	107.9	−15.1	1873
ChG-1_5.1	0.282159	0.000013	0.000135	0.000006	0.005260	0.000220	158.9	−18.2	2085
ChG-1_6.1	0.282402	0.000036	0.001010	0.000035	0.032200	0.001100	108.9	−10.8	1636
ChG-1_7.1	0.282286	0.000033	0.000975	0.000032	0.031050	0.000780	111.7	−14.8	1861
ChG-1_8.1	0.281290	0.000027	0.000292	0.000004	0.010740	0.000190	1958.0	−9.2	2998
ChG-1_9.1	0.282260	0.000019	0.000755	0.000014	0.026560	0.000510	108.3	−15.8	1912
ChG-1_10.1	0.282251	0.000019	0.000599	0.000019	0.018250	0.000220	108.2	−16.1	1929
ChG-1_11.1	0.282310	0.000019	0.000503	0.000012	0.017490	0.000470	111.5	−13.9	1813
ChG-1_12.1	0.282306	0.000023	0.000953	0.000045	0.025880	0.000780	109.6	−14.1	1823
ChG-1_13.1	0.282387	0.000023	0.000724	0.000048	0.023700	0.001700	109.5	−11.3	1664
ChG-1_14.1	0.281048	0.000018	0.000329	0.000003	0.010020	0.000110	2373.0	−8.4	3285
ChG-1_15.1	0.282245	0.000022	0.000472	0.000008	0.016680	0.000300	110.1	−16.3	1940
ChG-1_16.1	0.282347	0.000020	0.000620	0.000010	0.019310	0.000420	107.8	−12.7	1742
ChG-1_17.1	0.281422	0.000025	0.000914	0.000012	0.031920	0.000310	817.4	−30.3	3247
ChG-1_18.1	0.282329	0.000026	0.001150	0.000110	0.036400	0.002500	109.1	−13.4	1779
ChG-1_19.1	0.281330	0.000021	0.000571	0.000026	0.016770	0.000270	1682.0	−14.3	3056
ChG-1_20.1	0.282313	0.000026	0.001028	0.000043	0.039500	0.001500	108.5	−13.9	1810
ChG-1_21.1	0.280750	0.000017	0.000472	0.000010	0.016070	0.000220	2728.0	−11.2	3712
ChG-1_22.1	0.281125	0.000018	0.000515	0.000010	0.016960	0.000390	2162.0	−10.7	3243
ChG-1_23.1	0.282172	0.000018	0.000419	0.000005	0.013480	0.000140	185.4	−17.2	2051
ChG-1_24.1	0.282186	0.000019	0.000629	0.000006	0.021200	0.000320	165.9	−17.2	2033
ChG-1_25.1	0.282190	0.000016	0.000597	0.000007	0.019110	0.000350	164.3	−17.0	2025
ChG-1_26.1	0.282319	0.000019	0.000436	0.000003	0.015990	0.000150	110.2	−13.6	1795
ChG-1_27.1	0.282280	0.000017	0.000236	0.000003	0.008010	0.000110	816.6	0.5	1571
ChG-1_28.1	0.282298	0.000027	0.000838	0.000027	0.029060	0.000820	109.5	−14.4	1838
ChG-1_29.1	0.282452	0.000052	0.001504	0.000071	0.037700	0.001600	108.9	−9.0	1539
ChG-1_30.1	0.281521	0.000022	0.000633	0.000033	0.025200	0.001200	1273.0	−16.6	2862
ChG-1_31.1	0.282405	0.000018	0.000223	0.000004	0.008143	0.000095	106.7	−10.7	1628
ChG-1_32.1	0.282273	0.000019	0.000598	0.000014	0.018620	0.000240	108.4	−15.3	1886
ChG-1_33.1	0.282177	0.000016	0.000126	0.000004	0.004820	0.000120	163.1	−17.5	2049
ChG-1_34.1	0.281270	0.000017	0.000291	0.000004	0.010730	0.000120	1782.0	−13.8	3111

Table A3. *Cont.*

Spot No.	$^{176}Hf/^{177}Hf$	±2 s.d.	$^{176}Lu/^{177}Hf$	±2 s.d.	$^{176}Yb/^{177}Hf$	±2 s.d.	Apparent Age (Ma)	$\varepsilon_{Hf}(t)$	T_{2DM} (Ma)
Chilgok Formation									
ChG-1_35.1	0.281345	0.000022	0.000687	0.000023	0.025600	0.001000	1659.0	−14.4	3044
ChG-1_36.1	0.282272	0.000020	0.000450	0.000004	0.016140	0.000170	106.9	−15.4	1889
ChG-1_37.1	0.282285	0.000020	0.000564	0.000004	0.019660	0.000210	104.5	−15.0	1865
ChG-1_38.1	0.282279	0.000026	0.000706	0.000005	0.025350	0.000120	109.9	−15.1	1875
ChG-1_39.1	0.282293	0.000020	0.000510	0.000007	0.017840	0.000270	107.6	−14.6	1847
Silla Conglomerate									
Sila14_1.1	0.281677	0.000030	0.001728	0.000041	0.047390	0.000620	1833.7	0.0	2406
Sila14_2.1	0.282044	0.000022	0.000401	0.000005	0.010600	0.000200	165.0	−22.2	2308
Sila14_3.1	0.281529	0.000020	0.000313	0.000010	0.008740	0.000300	1848.1	−3.2	2590
Sila14_4.1	0.282535	0.000034	0.001451	0.000035	0.035180	0.000830	835.0	9.3	1101
Sila14_5.1	0.282258	0.000022	0.000570	0.000006	0.014860	0.000150	174.4	−14.4	1888
Sila14_6.1	0.282177	0.000034	0.001513	0.000024	0.044700	0.001200	780.8	−4.6	1823
Sila14_7.1	0.282280	0.000023	0.000793	0.000006	0.019900	0.000300	111.3	−15.0	1872
Sila14_8.1	0.281670	0.000020	0.000355	0.000002	0.009775	0.000080	1841.7	1.6	2325
Sila14_9.1	0.280592	0.000027	0.000884	0.000006	0.023810	0.000140	2042.7	−32.9	4323
Sila14_10.1	0.282073	0.000024	0.000398	0.000006	0.009810	0.000210	164.3	−21.2	2252
Sila14_11.1	0.282438	0.000029	0.000494	0.000005	0.010660	0.000200	798.4	5.5	1277
Sila14_12.1	0.281748	0.000028	0.000260	0.000004	0.007000	0.000200	1304.9	−7.5	2396
Sila14_13.1	0.282100	0.000032	0.001377	0.000030	0.036300	0.001400	789.6	−7.1	1965
Sila14_14.1	0.281330	0.000021	0.000319	0.000005	0.009590	0.000170	1038.3	−28.3	3312
Sila14_15.1	0.282126	0.000025	0.000692	0.000032	0.016390	0.000630	163.6	−19.3	2151
Sila14_16.1	0.282292	0.000029	0.001516	0.000039	0.040920	0.000750	113.9	−14.6	1850
Sila14_17.1	0.280595	0.000027	0.000283	0.000000	0.008069	0.000078	2539.6	−20.6	4064
Sila14_18.1	0.282044	0.000022	0.000541	0.000001	0.015910	0.000140	1217.5	0.8	1873
Sila14_19.1	0.282300	0.000022	0.000331	0.000003	0.008070	0.000110	823.4	1.3	1532
Sila14_20.1	0.282515	0.000051	0.001089	0.000050	0.026480	0.000880	107.2	−6.8	1415
Sila14_21.1	0.282455	0.000071	0.000759	0.000006	0.021550	0.000150	1352.7	18.2	1027
Sila14_22.1	0.282162	0.000025	0.000581	0.000011	0.014050	0.000250	114.4	−19.1	2100
Sila14_23.1	0.282474	0.000016	0.000267	0.000008	0.006710	0.000210	237.9	−5.4	1437
KU5_1.1	0.282251	0.000022	0.000490	0.000011	0.011600	0.000250	181.9	−14.5	1898
KU5_2.1	0.281786	0.000022	0.000728	0.000036	0.018800	0.001000	1919.0	7.0	2095
KU5_3.1	0.281679	0.000029	0.000500	0.000002	0.012936	0.000084	1879.0	2.6	2302
KU5_4.1	0.281381	0.000018	0.000755	0.000012	0.017550	0.000260	2177.0	−1.7	2769
KU5_5.1	0.282138	0.000021	0.000602	0.000008	0.013200	0.000280	1159.0	2.8	1717

Table A3. *Cont.*

Spot No.	$^{176}Hf/^{177}Hf$	±2 s.d.	$^{176}Lu/^{177}Hf$	±2 s.d.	$^{176}Yb/^{177}Hf$	±2 s.d.	Apparent Age (Ma)	$\varepsilon_{Hf}(t)$	T_{2DM} (Ma)
Silla Conglomerate									
KU5_6.1	0.282049	0.000019	0.000683	0.000006	0.015666	0.000085	394.3	−17.1	2206
KU5_7.1	0.282484	0.000024	0.001482	0.000014	0.034230	0.000270	228.2	−5.4	1431
KU5_8.1	0.281904	0.000023	0.001496	0.000015	0.037270	0.000510	760.1	−14.7	2359
KU5_9.1	0.281419	0.000024	0.000360	0.000006	0.009060	0.000130	2091.0	−1.7	2701
KU5_10.1	0.281345	0.000029	0.000175	0.000017	0.004480	0.000380	2067.0	−4.6	2839
KU5_11.1	0.282237	0.000023	0.000473	0.000021	0.011210	0.000480	172.2	−15.2	1930
KU5_12.1	0.282079	0.000018	0.000433	0.000004	0.010050	0.000091	166.5	−20.9	2239
KU5_13.1	0.281379	0.000025	0.000748	0.000013	0.017010	0.000260	2527.0	6.2	2630
KU5_14.1	0.282030	0.000021	0.000602	0.000007	0.014210	0.000180	184.9	−22.3	2328
KU5_15.1	0.281883	0.000026	0.000510	0.000007	0.013770	0.000270	1208.0	−5.1	2188
KU5_16.1	0.282177	0.000034	0.000421	0.000007	0.009020	0.000140	186.4	−17.0	2040
KU5_17.1	0.282066	0.000018	0.000311	0.000004	0.006837	0.000062	165.4	−21.4	2264
KU5_18.1	0.281611	0.000024	0.000419	0.000007	0.010690	0.000200	1883.0	0.4	2425
KU5_19.1	0.281267	0.000024	0.000238	0.000002	0.006126	0.000045	2398.0	0.1	2851
KU5_20.1	0.282323	0.000019	0.000227	0.000032	0.005800	0.000780	385.2	−7.5	1670
KU5_21.1	0.282477	0.000028	0.000700	0.000023	0.017570	0.000550	178.3	−6.6	1459
KU5_22.1	0.282137	0.000034	0.001606	0.000066	0.040300	0.001900	119.1	−20.0	2151
KU5_23.1	0.282089	0.000035	0.000760	0.000020	0.017310	0.000580	111.4	−21.8	2244
KU5_24.1	0.281295	0.000020	0.000381	0.000003	0.009294	0.000053	2376.0	0.4	2820
KU5_25.1	0.282264	0.000020	0.000847	0.000015	0.020170	0.000370	108.4	−15.7	1905
KU5_26.1	0.281950	0.000025	0.000466	0.000005	0.012620	0.000200	1014.4	−7.0	2137
KU5_27.1	0.281451	0.000018	0.000273	0.000015	0.006910	0.000370	1919.0	−4.3	2706
KU5_28.1	0.282163	0.000027	0.000465	0.000004	0.012230	0.000130	1152.0	3.6	1666
KU5_29.1	0.282088	0.000019	0.000079	0.000003	0.002275	0.000085	882.5	−4.8	1912
KU5_30.1	0.282308	0.000019	0.000502	0.000010	0.011900	0.000180	104.8	−14.1	1819
KU5_31.2	0.282160	0.000018	0.000433	0.000010	0.010020	0.000280	182.5	−17.7	2075
KU5_33.1	0.282173	0.000030	0.000738	0.000025	0.018990	0.000710	181.5	−17.3	2052
KU5_34.1	0.282157	0.000016	0.000379	0.000003	0.007990	0.000093	168.9	−18.1	2086
KU5_35.1	0.282296	0.000022	0.001085	0.000003	0.025930	0.000059	191.5	−12.8	1811
KU5_37.1	0.282108	0.000026	0.000510	0.000006	0.011940	0.000150	109.6	−21.1	2207
KU5_38.1	0.281288	0.000021	0.000322	0.000003	0.007504	0.000069	2582.0	4.9	2741
KU5_39.1	0.282111	0.000021	0.000718	0.000008	0.017670	0.000160	392.0	−15.0	2087
KU5_40.1	0.282180	0.000024	0.000536	0.000009	0.012690	0.000170	169.6	−17.3	2042
KU5_41.1	0.282213	0.000021	0.000510	0.000009	0.011430	0.000160	109.7	−17.4	2003

Table A3. *Cont.*

Spot No.	$^{176}Hf/^{177}Hf$	±2 s.d.	$^{176}Lu/^{177}Hf$	±2 s.d.	$^{176}Yb/^{177}Hf$	±2 s.d.	Apparent Age (Ma)	$\varepsilon_{Hf}(t)$	T_{2DM} (Ma)
Haman Formation.									
HA-1_1.1	0.282117	0.000033	0.000341	0.000017	0.008450	0.000420	110.3	−20.8	2189
HA-1_2.1	0.282295	0.000021	0.000519	0.000013	0.013260	0.000390	111.5	−14.5	1842
HA-1_3.1	0.282289	0.000018	0.000443	0.000002	0.011414	0.000072	110.2	−14.7	1854
HA-1_4.1	0.282313	0.000022	0.000934	0.000019	0.022740	0.000450	109.2	−13.9	1809
HA-1_5.1	0.281559	0.000019	0.000267	0.000013	0.007550	0.000330	1865.9	−1.7	2522
HA-1_6.1	0.282114	0.000030	0.000575	0.000016	0.013990	0.000270	114.7	−20.8	2193
HA-1_7.1	0.282232	0.000031	0.001161	0.000051	0.028600	0.001300	113.9	−16.7	1966
HA-1_8.1	0.282159	0.000027	0.000560	0.000014	0.012430	0.000230	116.2	−19.2	2105
HA-1_9.1	0.282118	0.000027	0.001170	0.000007	0.028080	0.000310	116.1	−20.7	2187
HA-1_10.1	0.282156	0.000028	0.000854	0.000009	0.021320	0.000500	116.4	−19.3	2112
HA-1_11.1	0.282299	0.000023	0.000685	0.000008	0.017510	0.000100	174.0	−13.0	1809
HA-1_12.1	0.282309	0.000035	0.000949	0.000011	0.025730	0.000150	172.4	−12.7	1792
HA-1_13.1	0.282139	0.000022	0.000640	0.000005	0.016340	0.000330	115.6	−19.9	2145
HA-1_14.1	0.282122	0.000024	0.000754	0.000028	0.017790	0.000540	117.4	−20.5	2177
HA-1_15.1	0.282111	0.000024	0.000893	0.000026	0.022620	0.000410	114.9	−20.9	2200
HA-1_16.1	0.282269	0.000028	0.000778	0.000015	0.020280	0.000420	113.0	−15.4	1893
HA-1_17.1	0.282325	0.000021	0.000547	0.000004	0.014827	0.000086	111.4	−13.4	1783
HA-1_18.1	0.282250	0.000019	0.000530	0.000006	0.012680	0.000220	114.3	−16.0	1929
HA-1_19.1	0.282189	0.000020	0.000710	0.000005	0.016850	0.000160	112.3	−18.2	2049
HA-1_20.1	0.282312	0.000018	0.000498	0.000011	0.013030	0.000370	114.3	−13.8	1808
HA-1_21.1	0.282297	0.000021	0.000766	0.000008	0.020380	0.000140	111.6	−14.4	1839
HA-1_22.1	0.282047	0.000024	0.000812	0.000005	0.020140	0.000210	115.7	−23.2	2324
HA-1_23.1	0.282217	0.000025	0.000721	0.000008	0.018540	0.000360	111.6	−17.2	1995
HA-1_24.1	0.282145	0.000021	0.000722	0.000010	0.017300	0.000240	113.8	−19.7	2134
HA-1_25.1	0.282325	0.000020	0.000528	0.000004	0.013239	0.000074	109.1	−13.5	1784
HA-1_26.1	0.282146	0.000019	0.000457	0.000004	0.012290	0.000110	113.5	−19.7	2131
HA-1_27.1	0.282233	0.000019	0.000440	0.000008	0.010670	0.000240	114.0	−16.6	1962
HA-1_28.1	0.282066	0.000017	0.000124	0.000009	0.003230	0.000250	118.0	−22.4	2284
HA-1_29.1	0.282309	0.000020	0.000703	0.000010	0.018820	0.000280	171.2	−12.7	1791
HA-1_30.1	0.282208	0.000019	0.000734	0.000011	0.017320	0.000240	112.4	−17.5	2012
HA-1_31.1	0.281463	0.000019	0.000588	0.000017	0.016280	0.000480	1973.8	−3.1	2683
HA-1_32.1	0.282324	0.000028	0.000766	0.000008	0.020370	0.000220	111.9	−13.5	1786
HA-1_33.1	0.282462	0.000022	0.000602	0.000007	0.016830	0.000310	223.0	−6.2	1470
HA-1_34.1	0.282171	0.000029	0.000905	0.000021	0.022510	0.000350	116.7	−18.8	2083
HA-1_35.1	0.282145	0.000032	0.001017	0.000021	0.023630	0.000460	113.6	−19.8	2135

Table A3. *Cont.*

Spot No.	$^{176}Hf/^{177}Hf$	±2 s.d.	$^{176}Lu/^{177}Hf$	±2 s.d.	$^{176}Yb/^{177}Hf$	±2 s.d.	Apparent Age (Ma)	$\varepsilon_{Hf}(t)$	T_{2DM} (Ma)
				Haman Formation.					
HA-1_36.1	0.281523	0.000018	0.000912	0.000005	0.023930	0.000120	761.7	−27.9	3076
HA-1_37.1	0.282284	0.000019	0.000468	0.000005	0.012270	0.000200	109.7	−14.9	1864
HA-1_38.1	0.282411	0.000015	0.000256	0.000002	0.006100	0.000110	264.9	−7.0	1549
HA-1_39.1	0.281499	0.000018	0.000905	0.000006	0.025800	0.000150	1865.4	−4.6	2680
HA-1_40.1	0.282053	0.000037	0.000561	0.000009	0.015050	0.000280	116.1	−22.9	2311
HA-1_41.1	0.282175	0.000020	0.000693	0.000019	0.018010	0.000590	113.2	−18.7	2076
HA-1_42.1	0.282251	0.000023	0.000736	0.000058	0.020100	0.001500	108.3	−16.1	1930
HA-1_43.1	0.282101	0.000020	0.000670	0.000013	0.016680	0.000360	115.7	−21.2	2219
HA-1_44.1	0.281449	0.000017	0.001184	0.000012	0.034150	0.000380	1849.4	−7.1	2801
HA-1_45.1	0.282248	0.000024	0.000797	0.000009	0.019570	0.000190	116.9	−16.0	1932
HA-1_46.1	0.282118	0.000023	0.000499	0.000006	0.013220	0.000260	103.5	−20.9	2190
HA-1_47.1	0.282174	0.000036	0.000887	0.000041	0.021220	0.000830	114.6	−18.7	2078
HA-1_48.1	0.282353	0.000020	0.000674	0.000005	0.017000	0.000170	110.4	−12.4	1730
HA-1_49.1	0.281429	0.000018	0.000727	0.000053	0.019100	0.001400	1271.0	−20.0	3043
HA-1_50.1	0.282234	0.000023	0.001270	0.000031	0.033420	0.000610	112.7	−16.7	1963
HA-1_51.1	0.282289	0.000019	0.000560	0.000006	0.014680	0.000190	110.6	−14.7	1854
HA-1_52.1	0.282298	0.000019	0.000561	0.000005	0.014570	0.000170	110.2	−14.4	1837
HA-1_53.1	0.282246	0.000017	0.000410	0.000006	0.011370	0.000210	189.2	−14.5	1905
HA-1_54.1	0.282188	0.000018	0.000670	0.000014	0.015200	0.000250	187.5	−16.6	2020
HA-1_55.1	0.282128	0.000022	0.000977	0.000006	0.024660	0.000100	107.3	−20.5	2171
HA-1_56.1	0.282427	0.000019	0.000488	0.000008	0.013580	0.000330	217.0	−7.5	1540
HA-1_57.1	0.281195	0.000017	0.000639	0.000002	0.017185	0.000090	1906.8	−14.1	3224
HA-1_58.1	0.281417	0.000016	0.000201	0.000003	0.005326	0.000066	2459.0	6.9	2536
HA-1_59.1	0.282263	0.000021	0.000744	0.000010	0.020390	0.000200	437.1	−8.6	1773
HA-1_60.1	0.282154	0.000027	0.000792	0.000009	0.018830	0.000200	114.2	−19.4	2117
HA-1_61.1	0.281115	0.000019	0.000536	0.000002	0.014430	0.000110	1914.0	−16.7	3366
HA-1_62.1	0.282348	0.000022	0.000540	0.000009	0.014990	0.000220	222.1	−10.2	1693
HA-1_63.1	0.282420	0.000019	0.000628	0.000007	0.017530	0.000140	223.6	−7.6	1552
HA-1_64.1	0.281494	0.000015	0.000159	0.000009	0.004680	0.000220	1635.9	−9.0	2737
HA-1_65.1	0.282203	0.000028	0.000723	0.000034	0.017720	0.000970	184.8	−16.2	1992
HA-1_66.1	0.282053	0.000017	0.000438	0.000007	0.011220	0.000220	113.3	−23.0	2312
HA-1_67.1	0.282120	0.000021	0.000737	0.000010	0.017570	0.000130	106.9	−20.8	2186
HA-1_68.1	0.282160	0.000021	0.000717	0.000013	0.017770	0.000410	114.2	−19.2	2105
HA-1_69.1	0.282254	0.000025	0.000651	0.000014	0.018860	0.000530	216.9	−13.7	1879
HA-1_70.1	0.282315	0.000019	0.000514	0.000004	0.013730	0.000220	110.2	−13.8	1803

Table A3. *Cont.*

Spot No.	$^{176}Hf/^{177}Hf$	±2 s.d.	$^{176}Lu/^{177}Hf$	±2 s.d.	$^{176}Yb/^{177}Hf$	±2 s.d.	Apparent Age (Ma)	$\varepsilon_{Hf}(t)$	T_{2DM} (Ma)
Jindong Formation									
JD-2-1_1.1	0.282931	0.000030	0.001083	0.000043	0.024780	0.000780	103.0	7.8	595
JD-2-1_2.1	0.282820	0.000028	0.000787	0.000015	0.020350	0.000260	108.8	4.0	812
JD-2-1_3.1	0.282961	0.000017	0.000742	0.000006	0.017190	0.000080	270.3	12.5	467
JD-2-1_4.1	0.282536	0.000033	0.001196	0.000008	0.031390	0.000470	99.1	−6.3	1377
JD-2-1_5.1	0.282782	0.000026	0.001149	0.000031	0.029500	0.000500	108.3	2.6	889
JD-2-1_6.1	0.282807	0.000026	0.000714	0.000018	0.019030	0.000320	105.6	3.5	839
JD-2-1_7.1	0.282801	0.000028	0.000921	0.000049	0.022070	0.000900	102.8	3.2	852
JD-2-1_8.1	0.282780	0.000025	0.001321	0.000042	0.034000	0.001000	102.8	2.4	895
JD-2-1_9.1	0.282943	0.000020	0.000762	0.000019	0.019480	0.000520	270.6	11.9	502
JD-2-1_10.1	0.282913	0.000019	0.000565	0.000004	0.013550	0.000210	277.9	11.0	557
JD-2-1_11.1	0.282951	0.000030	0.000878	0.000014	0.022230	0.000420	104.2	8.6	554
JD-2-1_12.1	0.282963	0.000035	0.001656	0.000027	0.043590	0.000640	273.0	12.5	471
JD-2-1_13.1	0.282972	0.000047	0.001413	0.000046	0.034300	0.001500	103.7	9.3	515
JD-2-1_14.1	0.282952	0.000026	0.000678	0.000010	0.016980	0.000250	271.4	12.2	483
JD-2-1_15.1	0.282920	0.000024	0.000409	0.000012	0.008660	0.000210	294.5	11.6	535
JD-2-1_16.1	0.282888	0.000030	0.001409	0.000007	0.038820	0.000200	107.3	6.4	680
JD-2-1_17.1	0.282545	0.000032	0.001014	0.000030	0.027530	0.000500	100.3	−5.9	1358
JD-2-1_18.1	0.282878	0.000023	0.000939	0.000017	0.022240	0.000240	102.0	5.9	700
JD-2-1_19.1	0.282981	0.000028	0.001083	0.000034	0.029200	0.001200	271.6	13.2	430
JD-2-1_20.1	0.281944	0.000030	0.001001	0.000016	0.026730	0.000280	109.2	−27.0	2526
JD-2-1_21.1	0.282932	0.000019	0.000465	0.000002	0.012033	0.000085	264.7	11.4	524
JD-2-1_22.1	0.282976	0.000036	0.001170	0.000030	0.027500	0.001000	283.5	13.2	436
JD-2-1_23.1	0.282500	0.000026	0.001049	0.000016	0.028220	0.000430	98.8	−7.5	1448
JD-2-1_24.1	0.282942	0.000023	0.001111	0.000012	0.027330	0.000150	300.0	12.4	496
JD-2-1_25.1	0.282933	0.000024	0.001077	0.000015	0.027150	0.000350	275.8	11.6	523
JD-2-1_26.1	0.282901	0.000015	0.000567	0.000029	0.012920	0.000500	234.2	9.6	599
JD-2-1_27.1	0.282532	0.000028	0.001106	0.000034	0.027700	0.000660	98.5	−6.4	1385
JD-2-1_28.1	0.282991	0.000038	0.001822	0.000009	0.043230	0.000210	290.0	13.8	411

References

1. Meng, Q.-R.; Zhang, G.-W. Timing of collision of the North and South China blocks: Controversy and reconciliation. *Geology* **1999**, *27*, 123–126. [CrossRef]
2. Kusky, T.M.; Windley, B.F.; Zhai, M.-G. Tectonic evolution of the North China Block: From orogen to craton to orogeny. In *Mesozoic Sub-Continental Lithospheric Thinning under Eastern Asia*; Zhai, M.-G., Windley, B.F., Kusky, T.M., Meng, Q.R., Eds.; Geological Society, Special Publications: London, UK, 2007; Volume 280, pp. 1–34.
3. Kinoshita, O. Migration of igneous activities related to ridge subduction in Southwest Japan and the East Asian continental margin from the Mesozoic to the Paleogene. *Tectonophysics* **1995**, *245*, 25–35. [CrossRef]
4. Li, Z.-X.; Li, X.-H. Formation of the 1300-km-wide intracontinental orogen and postorogenic magmatic province in Mesozoic South China: A flat-slab subduction model. *Geology* **2007**, *35*, 179–182. [CrossRef]
5. Isozaki, Y.; Aoki, K.; Nakama, T.; Yanai, S. New insight into a subduction-related orogen: A reappraisal of the geotectonic framework and evolution of the Japanese Islands. *Gondwana Res.* **2010**, *18*, 82–105. [CrossRef]
6. Isozaki, Y.; Itaya, T. Chronology of Sanbagawa metamorphism. *J. Metamorph. Geol.* **1990**, *8*, 401–411. [CrossRef]
7. Takasu, A.; Wallis, S.R.; Banno, S.; Dallmeyer, R.D. Evolution of the Sambagawa metamorphic belt, Japan. *Lithos* **1994**, *33*, 119–133. [CrossRef]
8. Aoya, M. P–T–D Path of eclogite from the Sambagawa belt deduced from combination of petrological and microstructural analyses. *J. Petrol.* **2001**, *42*, 1225–1248. [CrossRef]
9. Lee, D.-W. Strike–slip fault tectonics and basin formation during the Cretaceous in the Korean Peninsula. *Isl. Arc* **1999**, *8*, 218–231. [CrossRef]
10. Takashima, R.; Kawabe, F.; Nishi, H.; Moriya, K.; Wani, R.; Ando, H. Geology and stratigraphy of forearc basin sediments in Hokkaido, Japan: Cretaceous environmental events on the north-west Pacific margin. *Cretac. Res.* **2004**, *25*, 365–390. [CrossRef]
11. Lee, T.-H.; Park, K.-H.; Yi, K. SHRIMP U-Pb ages of detrital zircons from the early Cretaceous Nakdong Formation, SE Korea: Initiation of non-marine basin development and tectonic inversion. *Isl. Arc* **2018**, *27*, e12258. [CrossRef]
12. Isozaki, Y.; Ehiro, M.; Nakahata, H.; Aoki, K.; Sakata, S.; Hirata, T. Cambrian plutonism in Northeast Japan and its significance for the earliest arc-trench system of proto-Japan: New U–Pb zircon ages of the oldest granitoids in the Kitakami and Ou Mountains. *J. Asian Earth Sci.* **2015**, *108*, 136–149. [CrossRef]
13. Maruyama, S. Pacific-type orogeny revisited: Miyashiro-type orogeny proposed. *Isl. Arc* **1997**, *6*, 91–120. [CrossRef]
14. Nakajima, T. The Ryoke plutonometamorphic belt: Crustal section of the Cretaceous Eurasian continental margin. *Lithos* **1994**, *33*, 51–66. [CrossRef]
15. Aoki, K.; Isozaki, Y.; Yamamoto, S.; Maki, K.; Yokoyama, T.; Hirata, T. Tectonic erosion in a Pacific-type orogen: Detrital zircon response to Cretaceous tectonics in Japan. *Geology* **2012**, *40*, 1087–1090. [CrossRef]
16. Sagong, H.; Kwon, S.-T. Mesozoic episodic magmatism in South Korea and its tectonic implication. *Tectonics* **2005**, 24. [CrossRef]
17. Park, K.-H. Cyclic igneous activities during the Late Paleozoic to Early Cenozoic period over the Korean peninsula. *J. Petrol. Soc. Korea* **2012**, *21*, 193–202. [CrossRef]
18. Kiminami, K.; Imaoka, T. Spatiotemporal variations of Jurassic–Cretaceous magmatism in eastern Asia (Tan-Lu Fault to SW Japan): Evidence for flat-slab subduction and slab rollback. *Terra Nova* **2013**, *25*, 414–422. [CrossRef]
19. Lee, T.-H.; Park, K.-H.; Yi, K. Nature and evolution of the Cretaceous basins in the eastern margin of Eurasia: A case study of the Gyeongsang Basin, SE Korea. *J. Asian Earth Sci.* **2018**, *166*, 19–31. [CrossRef]
20. Aoki, K.; Isozaki, Y.; Kofukuda, D.; Sato, T.; Yamamoto, A.; Maki, K.; Hirata, T. Provenance diversification within an arc-trench system induced by batholith development: The Cretaceous Japan case. *Terra Nova* **2014**, *26*, 139–149. [CrossRef]
21. Iizuka, T.; Komiya, T.; Rino, S.; Maruyama, S.; Hirata, T. Detrital zircon evidence for Hf isotopic evolution of granitoid crust and continental growth. *Geochim. Cosmochim. Acta* **2010**, *74*, 2450–2472. [CrossRef]
22. Asiedu, D.K.; Suzuki, S.; Shibata, T. Provenance of sandstones from the Wakino Subgroup of the Lower Cretaceous Kanmon Group, northern Kyushu, Japan. *Isl. Arc* **2000**, *9*, 128–144. [CrossRef]

23. Saito, M.; Takarada, S.; Toshimitsu, S.; Mizuno, K.; Miyazaki, K.; Hoshizumi, H.; Hamasaki, S.; Sagaguchi, K.; Ohno, T.; Murata, Y. Yatsushiro and a part of Nomo Zaki. In *Geological Map of Japan 1:200,000 NI-52-12, 18*; Geological Survey of Japan: Tokyo, Japan, 2010.
24. Komatsu, T.; Naruse, H.; Manabe, M.; Tsuihiji, T.; Ikegami, N.; Takashima, R. Cretaceous non-marine and shallow marine facies and fossils in western Kumamoto, Kyushu, Japan. Field Excursion Guidebook. In Proceedings of the 4th International Symposium, IGCP507, Paleoclimates of the Cretaceous in Asia and their Global Correlation, Kumamoto, Japan, 1–6 December 2009.
25. Tsutsumi, Y.; Miyake, Y.; Komatsu, T. Depositional age of the Himenoura Group on the Amakusa-Kamishima area, Kyushu, southwest Japan: U sing zircon U–Pb dating of the acidic tuffs. *Isl. Arc* **2017**, *26*, e12194. [CrossRef]
26. Kikuchi, N.; Tashiro, M. Trigonioides (Cretaceous non-marine bivalves) from the Goshoura Group in Kyushu. *Mem. Fac. Sci. Kochi Univ. Ser. E Geol.* **1999**, *19*, 23–31.
27. Komatsu, T.; Jinhua, C.; Ugai, H.; Hirose, K. Notes on non-marine bivalve Trigonioides (Trigonioides?) from the mid-Cretaceous Goshoura Group, Kyushu, Japan. *J. Asian Earth Sci.* **2007**, *29*, 795–802. [CrossRef]
28. Komatsu, T.; Ono, M.; Naruse, H.; Kumagae, T. Upper Cretaceous depositional environments and bivalve assemblages of far-east Asia: The Himenoura Group, Kyushu, Japan. *Cretac. Res.* **2008**, *29*, 489–508. [CrossRef]
29. Kojo, Y.; Komatsu, T.; Iwamoto, T.; Takashima, R.; Takahashi, O.; Nishi, H. Stratigraphy and detailed age of the Upper Cretaceous Himenoua Group in the eastern part of Amakusa-Kamishima Island, Kumamoto, Japan. *J. Geol. Soc. Japan* **2011**, *117*, 398–416. [CrossRef]
30. Chang, K.H. Cretaceous stratigraphy of southeast Korea. *J. Geol. Soc. Korea* **1975**, *11*, 1–23.
31. Chang, K.H. Late Mesozoic stratigraphy, sedimentation and tectonics of southeastern Korea. *J. Geol. Soc. Korea* **1977**, *13*, 76–90, (in Korean with English abstract).
32. Chough, S.K.; Sohn, Y.K. Tectonic and sedimentary evolution of a Cretaceous continental arc–backarc system in the Korean peninsula: New view. *Earth Sci. Rev.* **2010**, *101*, 225–249. [CrossRef]
33. Chang, K.H.; Kim, H.M. Cretaceous paleocurrent and sedimentation in northwestern part of Gyeongsang Basin, southern Korea. *J. Geol. Soc. Korea* **1968**, *4*, 77–97.
34. Chang, K.H. Cretaceous stratigraphy and paleocurrent analysis of Kyongsang Basin, Korea. *J. Geol. Soc. Korea* **1988**, *24*, 194–205.
35. Kim, H.M. Paleocurrent analysis and depositional history of the Cretaceous Jinju Formation in Jinju-Sacheon area, Korea. *J. Geol. Soc. Korea* **1994**, *30*, 506–519, (in Korean with English abstract).
36. Cheong, D.K.; Kim, Y.I. Sedimentological study of the Nakdong Formation to analyse the forming and evolving tectonics of the Cretaceous Gyeongsang Basin, I: Depositional setting, source, and paleocurrent analyses of the Nakdong Formation in the southwestern Gyeongsang Basin. *Econ. Environ. Geol.* **1996**, *29*, 639–660, (in Korean with English abstract).
37. Chang, K.H.; Woo, B.G.; Lee, J.H.; Park, S.O.; Yao, A. Cretaceous and Early Cenozoic stratigraphy and history of eastern Kyongsang Basin, S. *Korea. J. Geol. Soc. Korea* **1990**, *26*, 471–487.
38. Mitsugi, T.; Ishida, K.; Woo, B.-G.; Chang, K.-H.; Park, S.-O.; Hirano, H. Radiolarian-brearing conglomerate from the Hayang Group, the Kyongsang Supergroup, southeastern Korea. *J. Asian Earth Sci.* **2001**, *19*, 751–753. [CrossRef]
39. Sohn, Y.K.; Son, M.; Jeong, J.O.; Jeon, Y.M. Eruption and emplacement of a laterally extensive, crystal-rich, and pumice-free ignimbrite (the Cretaceous Kudsandong Tuff, Korea). *Sediment. Geol.* **2009**, *220*, 190–203. [CrossRef]
40. Paces, J.B.; Miller, J.D., Jr. Precise U-Pb ages of Duluth complex and related mafic intrusions, northeastern Minnesota: Geochronological insights to physical, petrogenetic, paleomagnetic, and tectonomagmatic processes associated with the 1.1 Ga midcontinent rift system. *J. Geophys. Res. Solid Earth* **1993**, *98*, 13997–14013. [CrossRef]
41. Ludwig, K.R. *SQUID 2: A User's Manual*; Berkeley Geochronology Center: Berkeley, CA, USA, 2009; Volume 5, p. 110.
42. Ludwig, K.R. *User's Manual for Isoplot 3.7*; Berkeley Geochronology Center: Berkeley, CA, USA, 2008; Volume 4, p. 70.
43. Iizuka, T.; Hirata, T. Improvements of precision and accuracy in in situ Hf isotope microanalysis of zircon using the laser ablation-MC-ICPMS technique. *Chem. Geol.* **2005**, *220*, 121–137. [CrossRef]
44. Chu, N.C.; Taylor, R.N.; Chavagnac, V.; Nesbitt, R.W.; Boella, R.M.; Milton, J.A.; Burton, K. Hf isotope ratio analysis using multi-collector inductively coupled plasma mass spectrometry: An evaluation of isobaric interference corrections. *J. Anal. Spectrom.* **2002**, *17*, 1567–1574. [CrossRef]

45. Vervoort, J.D.; Patchett, P.J.; Söderlund, U.; Baker, M. Isotopic composition of Yb and the determination of Lu concentrations and Lu/Hf ratios by isotope dilution using MC-ICPMS. Geochem. *Geophys. Geosyst.* **2004**, *5*, Q11002. [CrossRef]
46. Patchett, P.J.; Kouvo, O.; Hedge, C.E.; Tatsumoto, M. Evolution of continental crust and mantle heterogeneity: Evidence from Hf isotopes. *Contrib. Mineral. Petrol.* **1982**, *78*, 279–297. [CrossRef]
47. Paton, C.; Hellstrom, J.; Paul, B.; Woodhead, J.; Hergt, J. Iolite: Freeware for the visualisation and processing of mass spectrometric data. *J. Anal. Spectrom.* **2011**, *26*, 2508–2518. [CrossRef]
48. Griffin, W.L.; Wang, X.; Jackson, S.E.; Pearson, N.J.; O'Reilly, S.Y.; Xu, X.; Zhou, X. Zircon chemistry and magma mixing, SE China: In-situ analysis of Hf isotopes, Tonglu and Pingtan igneous complexes. *Lithos* **2002**, *61*, 237–269. [CrossRef]
49. Rudnick, R.L.; Gao, S. Composition of the continental crust. In *Treatise on Geochemistry, The Crust*; Rudnick, R.L., Ed.; Elsevier: New York, NY, USA, 2003; Volume 3, pp. 1–64.
50. Hoskin, P.W.O.; Schaltegger, U. The composition of zircon and igneous and metamorphic petrogenesis. *Rev. Mineral. Geochem.* **2003**, *53*, 27–62. [CrossRef]
51. Maki, K.; Yui, T.F.; Miyazaki, K.; Fukuyama, M.; Wang, K.L.; Martens, U.; Liou, J.G. Petrogenesis of metatexite and diatexite migmatites determined using zircon U–Pb age, trace element and Hf isotope data, Higo metamorphic terrane, central Kyushu, Japan. *J. Metamorph. Geol.* **2014**, *32*, 301–323. [CrossRef]
52. Sakashima, T.; Terada, K.; Takeshita, T.; Sano, Y. Large-scale displacement along the Median Tectonic Line, Japan: Evidence from SHRIMP zircon U–Pb dating of granites and gneisses from the South Kitakami and paleo-Ryoke belts. *J. Asian Earth Sci.* **2003**, *21*, 1019–1039. [CrossRef]
53. Kim, N.; Cheong, C.-S.; Park, K.-H.; Kim, J.; Song, Y.-S. Crustal evolution of northeastern Yeongnam Massif, Korea, revealed by SHRIMP U–Pb zircon geochronology and geochemistry. *Gondwana Res.* **2012**, *21*, 865–875. [CrossRef]
54. Cho, D.-L.; Lee, B.C.; Oh, C.W. Petrogenesis of paleoproterozoic (2.02–1.96 Ga) metagranitoids in the southwestern Yeongnam Massif, Korean Peninsula, and their significance for the tectonic history of northeast Asia: Insights from zircon U–Pb–Hf isotope and whole-rock geochemical compositions. *Precambrian Res.* **2020**, *340*, 105631.
55. Hisada, K.-I.; Takashima, S.; Arai, S.; Lee, Y.I. Early cretaceous paleogeography of Korea and Southwest Japan inferred from occurrence of detrital chromian spinels. *Isl. Arc* **2008**, *17*, 471–484. [CrossRef]
56. Ogasawara, M.; Fukuyama, M.; Horie, K. SHRIMP U–Pb zircon dating of the Kinshozan Quartz Diorite from the Kanto Mountains, Japan: Implications for late Paleozoic granitic activity in Japanese Islands. *Isl. Arc* **2016**, *25*, 28–42. [CrossRef]
57. Tsutsumi, Y.; Yokoyama, K.; Kasatkin, S.A.; Golozubov, V.V. Zircon U–Pb age of granitoids in the Maizuru Belt, southwest Japan and the southernmost Khanka Massif, Far East Russia. *J. Mineral. Petrol. Sci.* **2014**, *109*, 97–102. [CrossRef]
58. Takahashi, Y.; Cho, D.-L.; Mao, J.; Zhao, X.; Yi, K. SHRIMP U–Pb zircon ages of the Hida metamorphic and plutonic rocks, Japan: Implications for late Paleozoic to Mesozoic tectonics around the Korean Peninsula. *Isl. Arc* **2018**, 27. [CrossRef]
59. Park, K.-H.; Lee, T.-H. Characteristics of Nd Isotopic Compositions of the Phanerozoic Granitoids of Korea and Their Genetic Significance. *J. Petrol. Soc. Korea* **2014**, *23*, 279–292. [CrossRef]
60. Cheong, C.-S.; Yi, K.; Kim, N.; Lee, T.-H.; Lee, S.R.; Geng, J.-Z.; Li, H.-k. Tracking source materials of Phanerozoic granitoids in South Korea by zircon Hf isotopes. *Terra Nova* **2013**, *25*, 228–235. [CrossRef]
61. Kim, N.; Cheong, C.-S.; Yi, K.; Song, Y.-S.; Park, K.-H.; Geng, J.-Z.; Li, H.-k. Zircon U-Pb geochronological and Hf isotopic constraints on the Precambrian crustal evolution of the north-eastern Yeongnam Massif, Korea. *Precambrian Res.* **2014**, *242*, 1–21. [CrossRef]
62. Kim, M.J.; Ha, Y.; Choi, J.E.; Park, K.-H.; Song, Y.-S.; Liu, S. U-Pb ages and Hf isotopic compositions of detrital zircons from the Seochangni Formation of the northeastern Okcheon Metamorphic Belt: Implications to the crustal evolution of the Sino-Korean craton since Paleoproterozoic. *Lithos* **2020**. under review.
63. Osozawa, S.; Usukic, T.; Usukid, M.; Wakabayashie, J.; Jahn, B.-m. Trace elemental and Sr-Nd-Hf isotopic compositions, and U-Pb ages for the Kitakami adakitic plutons: Insights into interactions with the early Cretaceous TRT triple junction offshore Japan. *J. Asian Earth Sci.* **2019**, *184*, 103968. [CrossRef]
64. Tsuchiya, N.; Takeda, T.; Adachi, T.; Nakano, N.; Osanai, Y.; Adachi, Y. Early Cretaceous adakitic magmatism and tectonics in the Kitakami Mountains, Japan. *Jpn. Mag. Mineral. Petrol. Sci.* **2015**, *44*, 69–90.

65. Wu, F.-Y.; Han, R.-H.; Yang, J.-H.; Wilde, S.A.; Zhai, M.G.; Park, S.C. Initial constraints on the timing of granitic magmatism in North Korea using U–Pb zircon geochronology. *Chem. Geol.* **2007**, *238*, 232–248. [CrossRef]
66. Kim, S.W.; Ryu, I.-C.; Jeong, Y.-J.; Choi, S.-J.; Kee, W.-S.; Yi, K.; Lee, Y.S.; Kim, B.-C.; Park, D.W. Characteristics of the early cretaceous igneous activity in the korean peninsula and tectonic implications. *J. Geol.* **2012**, *120*, 625–646. [CrossRef]
67. Takahashi, Y.; Mikoshiba, M.; Kubo, K.; Iwano, H.; Danhara, T.; Hirata, T. Zircon U–Pb ages of plutonic rocks in the southern Abukuma Mountains: Implications for Cretaceous geotectonic evolution of the Abukuma Belt. *Isl. Arc* **2016**, *25*, 154–188. [CrossRef]
68. Li, X.-H.; Li, Z.-X.; Li, W.-X. Detrital zircon U–Pb age and Hf isotope constrains on the generation and reworking of Precambrian continental crust in the Cathaysia Block, South China: A synthesis. *Gondwana Res.* **2014**, *25*, 1202–1215. [CrossRef]
69. Jahn, B.M. Accretionary orogen and evolution of the Japanese Islands: Implications from a Sr-Nd isotopic study of the Phanerozoic granitoids from SW Japan. *Am. J. Sci.* **2010**, *310*, 1210–1249. [CrossRef]
70. Kinny, P.D.; Maas, R. Lu–Hf and Sm–Nd isotope systems in zircon. *Rev. Mineral. Geochem.* **2003**, *53*, 327–341. [CrossRef]
71. Drummond, M.S.; Defant, M.J.; Kepezhinskas, P.K. Petrogenesis of slab-derived trondhjemite-tonalite-dacite/adakite magmas. *Trans. R. Soc. Edinb. Earth Sci.* **1996**, *87*, 205–215.
72. Condie, K.C. TTGs and adakites: Are they both slab melts? *Lithos* **2005**, *80*, 33–44. [CrossRef]
73. Tang, G.-J.; Wang, Q.; Wyman, D.A.; Chung, S.-L.; Chen, H.-Y.; Zhao, Z.-H. Genesis of pristine adakitic magmas by lower crustal melting: A perspective from amphibole composition. *J. Geophys. Res. Solid Earth* **2017**, *122*, 1934–1948. [CrossRef]
74. Ribeiro, J.M.; Maury, R.C.; Grégoire, M. Are adakites slab melts or high-pressure fractionated mantle melts? *J. Petrol.* **2016**, *57*, 839–862. [CrossRef]
75. Zhu, D.-C.; Zhao, Z.-D.; Pan, G.-T.; Lee, H.-Y.; Kang, Z.-Q.; Liao, Z.-L.; Wang, L.-Q.; Li, G.-M.; Dong, G.-C.; Liu, B. Early cretaceous subduction-related adakite-like rocks of the Gangdese Belt, southern Tibet: Products of slab melting and subsequent melt–peridotite. *J. Asian Earth Sci.* **2009**, *34*, 298–309. [CrossRef]
76. Kamei, A. An adakitic pluton on Kyushu Island, southwest Japan arc. *J. Asian Earth Sci.* **2004**, *24*, 43–58. [CrossRef]
77. Mateen, T.; Okamoto, K.; Chung, S.-L.; Wang, K.-L.; Lee, H.-Y.; Abe, S.; Mita, Y.; Rehman, H.U.; Terabayashi, M.; Yamamoto, H. LA-ICP-MS zircon U-Pb age and Hf isotope data from the granitic rocks in the Iwakuni area, southwest Japan: Reevaluation of emplacement order and the source magma. *Geosci. J.* **2019**, *23*, 917–931. [CrossRef]
78. Kawaguchi, K.; Hayasaka, Y.; Shibata, T.; Komatsu, M.; Kimura, K.; Das, K. Discovery of Paleozoic rocks at northern margin of Sambagawa terrane, eastern Kyushu, Japan: Petrogenesis, U–Pb geochronology and its tectonic implication. *Geosci. Front.* **2020**, *11*, 1441–1459. [CrossRef]
79. Kamata, Y.; Hisada, K.-I.; Lee, Y.I. Late Jurassic radiolarians from pebbles of Lower Cretaceous conglomerates of the Hayang Group, southeastern Korea. *Geosci. J.* **2000**, *4*, 165–174. [CrossRef]

Publisher's Note: MDPI stays neutral with regard to jurisdictional claims in published maps and institutional affiliations.